PART-A

Designing of catalysts based on

Iron & Phosphomolybdic acid

CHAPTER 1

Cesium salt of iron substituted phosphomolybdate ($PMo_{11}Fe$):

Synthesis, characterization and application for hydrogenation of styrene

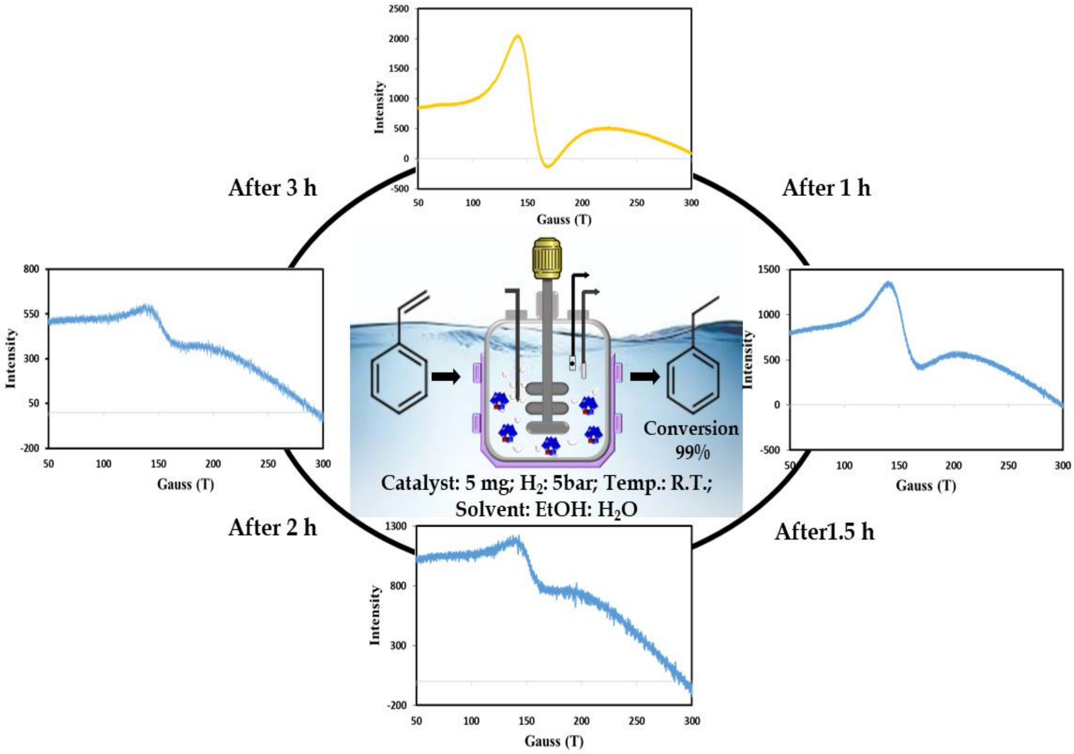

Molecular Catalysis 513 (2021) 111827

Contents lists available at ScienceDirect

Molecular Catalysis

journal homepage: www.journals.elsevier.com/molecular-catalysis

Cesium salt of iron substituted phosphomolybdate: Synthesis, characterization, room temperature hydrogenation of styrene and its mechanistic evaluation

Anjali U. Patel *, Jay R. Patel

Polyoxometalates and Catalysis Laboratory, Department of Chemistry, Faculty of Science, The Maharaja Sayajirao University of Baroda, Vadodara-390002, India

ARTICLE INFO

Keywords:
Iron substituted phosphomolybdate
Hydrogenation
Styrene
Water

ABSTRACT

The present article elucidates one-pot synthesis of Cs salt of iron substituted phosphomolybdate, its characterizations and application for styrene hydrogenation. The synthesized material was characterized by elemental analysis, TGA, FT-IR, FT-Raman, ESR, XPS and XRD. A detailed study was carried out for maximum conversion of styrene to ethylbenzene by optimizing different parameters such as solvent, catalyst amount, hydrogen pressure, time and temperature. The catalyst shows high efficiency (99% conversion) with low catalyst amount (5 mg, Fe: 0.02 mol%), EtOH: water (1:1) as green solvent, low pressure (5 bar) in EtOH: H_2O aqueous medium at room temperature only. The catalyst was easily recycled by simply centrifugation and reused for up to two cycles without any leaching or degradation. The present method is highly sustainable and green with no waste generation (E-factor = 0) with high Reaction mass efficiency (100%) as well as 100% atom economy. The role of water was confirmed by an isotope labeling experiment using D_2O as a solvent and a mechanistic study was investigated by ESR.

As mentioned in general introduction, transition metal substituted phosphomolybdate is most important due to its unique redox properties [1-4]. A literature survey shows that reports are available on first row 3d transition metals i.e., V [1, 5-10], Mn [2-4, 11, 12], Fe [7, 13-17], Co [2-4, 7, 11, 12, 15, 18-20], Ni [3, 4, 11, 15, 18, 20], Cu [11, 18, 20-22] and Zn [11] substituted phosphomolybdates and on catalytic activity for oxidation (styrene, alcohol and phenol), oxidative desulfurization and dye degradation reactions. Amongst all, Fe is found to the best candidate as it is very cheap, naturally abundant, non-toxic and has unique magnetic properties [23, 24].

In 2001, Mizuno et al. first time reported the synthesis of $Cs_3H_1PMo_{11}FeO_{39}$, $Cs_{1.5}Fe_{0.5}PMo_{12}O_{40}$, and $Cs_2(NH_4)_2PMo_{11.5}Fe_{0.5}O_{39}$, at pH 4.4 from $PMo_{12}O_{40}$ using lithium carbonate, followed by the addition of $Fe(NO_3)_3.9H_2O$ [13]. The synthesized complex was characterized by X-ray fluorescence, TGA, FT-IR, BET and XRD and its catalytic efficiency was evaluated for selective oxidation of isobutene. Further in 2004, Mizuno group synthesized $Cs_{2.8}H_{1.2}PMo_{11}Fe(H_2O)O_{39}.6H_2O$ at pH 4.3 using the same method which was reported earlier and characterized by EDX, TGA, FT-IR, ^{31}P NMR, ESR and XRD [14]. Its catalytic activity was evaluated for oxidative dehydrogenation of 2-propanol.

In 2009, Rabia group reported the synthesis of $(NH_4)_6HPMo_{11}Fe^{III}(H_2O)O_{39}$ from H_3PO_4, $(NH_4)_2Mo_2O_7$ and $Fe(NO_3)_3$ in which pH was maintained by using sulfuric acid and synthesis was carried out at 0 °C to avoid formation of 6-molybdometalate and NH_4NO_3 were added to precipitate of the complex and characterized by various analytical methods such as Elemental analysis, FT-IR, DRS, ^{31}P NMR and XRD [15]. The catalytic activity of the synthesized complex was evaluated for the oxidation of propene. Later, in 2015, Wang et al. reported the synthesis of $Na_6PMo_{11}FeO_{40}$ by adjusting pH 6 of phosphomolybdate solution using $NaHCO_3$, followed by the addition of iron nitrate solution and characterization by some basic techniques such as FT-IR and UV-Visible spectroscopy [16]. The synthesized complex was studied for its inhibitory effect on mushroom tyrosine and as a preventive measure against the peroxidation of fresh-cut fruits and vegetables.

In 2017, Rahimi et al. synthesized $Cs_4H_2PMo_{11}FeO_{40}.6H_2O$ using the same method reported by Mizuno group [14] and its catalytic efficiency was evaluated for selective adsorption of methylene blue dye form a mixture of organic dyes (methylene blue, methyl orange, and rhodamine-B)[17]. In 2019, Wang group studied the inhibition effect of α-glucosidase using transition metals (Fe, V and Co) substituted phosphomolybdate as inhibitors.

Thus, a literature survey shows that there is neither detailed characterization data for $PMo_{11}Fe$ nor any report available on hydrogenation of styrene using $PMo_{11}Fe$ even though the resulting product plays a pivotal role in the current chemical industries for triggering a wide range of substrates commonly used in the production of either intermediates or finished products. Hydrogenated product, ethylbenzene has been used in gasoline, paints, inks, insecticides, carpet glues [25, 26].

In this context, the present chapter describes one-pot synthesis of cesium salt of iron substituted phosphomolybdate and its detailed characterization by various techniques such as elemental analysis, TGA, FT-IR, Raman spectroscopy, ESR, XPS, ^{31}P MAS NMR and Powder XRD. Catalyst efficiency was evaluated for styrene hydrogenation in aqueous medium/ neat water under mild conditions using molecular H_2 as a reducing agent. Various parameters like catalyst to substrate ratio, pressure, solvent, time and temperature have been optimized for maximum % conversion. Also, heterogeneity test, recycling and reusability were studied under optimized conditions. The regenerated catalyst was characterized by EDX, FT-IR, Raman Spectroscopy and XPS to confirm the stability of the catalyst. Green chemistry matrices were calculated and catalytic activity of the present catalyst was also compared with reported iron-based catalysts. The possible reaction mechanism was investigated by ESR spectroscopy and D_2O NMR study.

EXPERIMENTAL

Materials

All chemicals used were of A.R. grade. Phosphomolybdic acid ($H_3PMo_{12}O_{40}$), iron nitrate [$(Fe(NO_3)_3).9H_2O$], Cesium chloride (CsCl), Sodium bicarbonate ($NaHCO_3$), styrene and dichloromethane (DCM)/ ethyl acetate were obtained from Merck and were used as received without further purification.

Synthesis of iron substituted phosphomolybdate

Cs salt of iron substituted phosphomolybdate was synthesized by the reported method [14] with some modifications, especially lithium carbonate is replaced by sodium bicarbonate. $H_3PM_{12}O_{40}$ (1.825 g, 1 mmol) was dissolved in a minimum quantity of water and pH= 4.3 was maintained by the addition of saturated sodium bicarbonate ($NaHCO_3$). The obtained solution was heated at 80 °C with stirring and to this, a saturated solution of $Fe(NO_3)_3.9H_2O$ ($Fe(NO_3)_3$: 0.404 gm, 1 mmol) in water, was added. The final pH of the resulting mixture was maintained at 4.3 by adding saturated $NaHCO_3$ solution, refluxed at 80 °C for 1 h and filtered hot. To this (filtrate), saturated CsCl (5 mmol, 0.8418 gm) solution was added and obtained yellow color precipitates were filtered, washed with water, dried at room temperature and designated as $PMo_{11}Fe$ (Scheme 1). The filtrate was used for estimation of molybdenum.

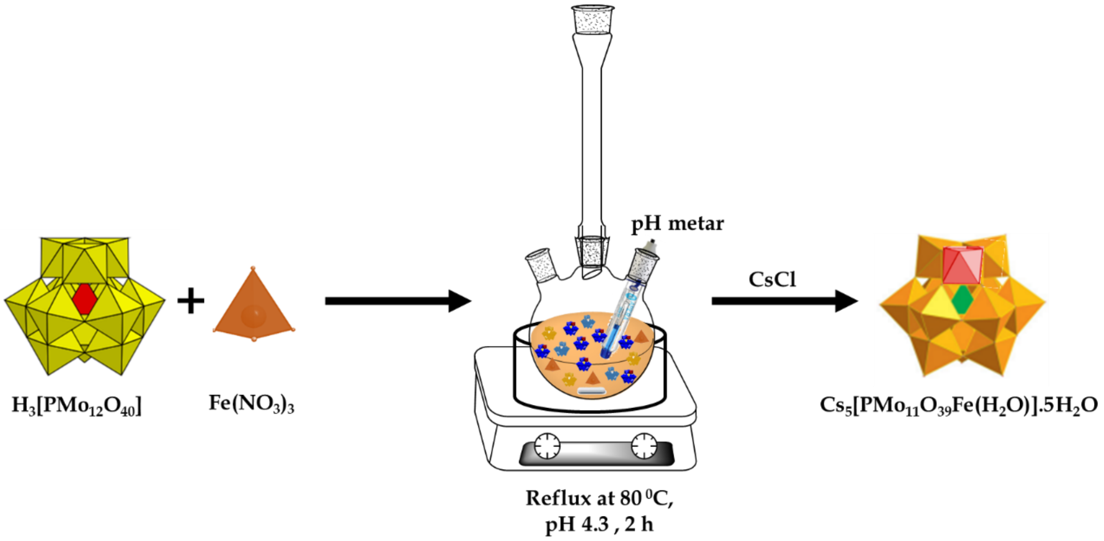

Scheme 1. One-pot synthesis of $PMo_{11}Fe$

Catalytic activity

Hydrogenation of styrene was carried out in the high pressure autoclave. The reaction vessel was charged with 10 mmol of styrene, 50 mL of ethanol: water (30:20 mL) as a solvent and 5 mg of catalyst. The presence of air in the unfilled space of the reactor vessel was removed by purging with H_2 gas several times. Finally for the reaction, 5 bar H_2 pressure was applied and set at 30 °C for 3 h with a stirring rate of 500 rpm. The progress of the reaction was demonstrated by a continuous decrease in pressure inside the reactor. After completion, the reaction mixture was cooled to room temperature and then H_2 pressure was released from the vent valve. The organic layer was extracted using dichloromethane, while the catalyst was collected from the junction of the liquid phases and finally recovered by centrifugation. The organic phase was dried with anhydrous magnesium sulfate and analyzed by a gas chromatograph (Shimadzu-2014) using a capillary column (RTX-5). The products were confirmed by comparison with the standard samples while conversion, selectivity, TON and TOF were calculated using equations given in general introduction. The schematic representation of catalytic methodology is represented in scheme 2.

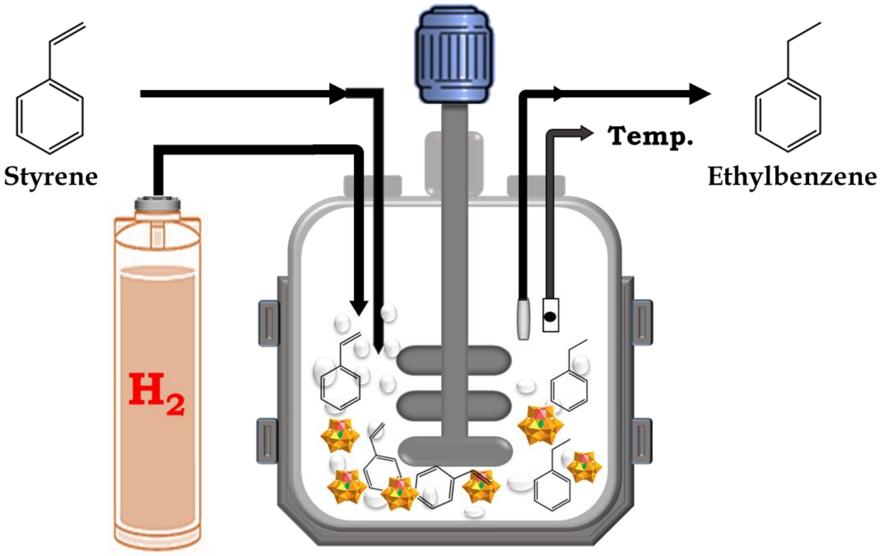

Scheme 2. Schematic illustration of the styrene hydrogenation reaction

Results and discussion

Please note that for $PMo_{11}Fe$, we have not synthesized Fe nano particles because reduction of Fe(3+) to Fe(0) requires high pressure, temperature and time. Under these conditions, PMo_{11} gets reduced with decomposing Keggin unit.

Characterization

Cesium salt of iron substituted phosphomolybdate was isolated and the remaining solution was filtered. The filtrate was analyzed for molybdenum gravimetrically [27]. The observed proportion of Mo in the filtrate was 5%, which corresponds to the loss of one equivalent of Mo from $H_3PMo_{12}O_{40}$.

Energy-dispersive X-ray mapping (EDX) shows (Figure 1) the presence of Cs, P, Mo, Fe and O in the synthesized materials. The observed EDX values of the elements (Cs:25.88%, P:1.27%, Mo:41.39%, Fe:2.08%, O:28.97%) were well consistent with the that of the calculated values (Cs:25.99%, P:1.21%, Mo: 41.28%, Fe:2.18%, O:28.79%). Further, ICP-AES analysis also confirmed that the P (1.36%), Mo (42.19%) and iron (2.75%) contents were present in synthesized material, which is in good agreement with the calculated one.

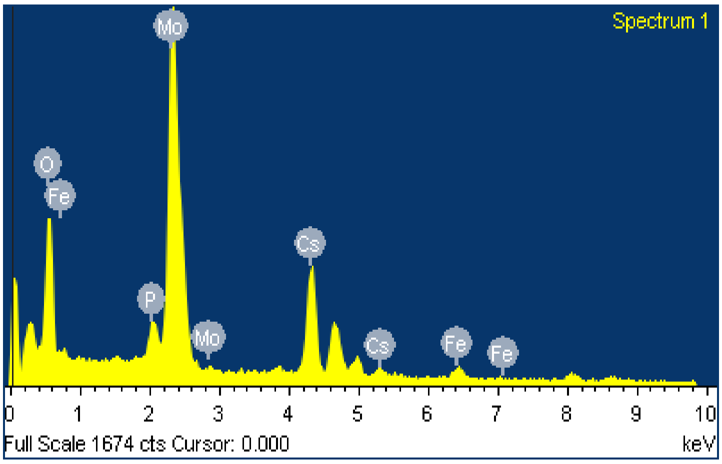

Figure 1. EDX mapping of $PMo_{11}Fe$

Thermogravimetric analysis (TGA) shows (Figure 2) an initial weight loss of 2.5% up to 100 °C, which is attributed to loss of adsorbed water. Further, 1.3% weight loss is observed between 150 - 350 °C because of water of crystallization. No other significant weight loss indicates that the synthesized material is stable up to 500 °C. Based on the total weight loss, the number of water molecules was calculated using the formula $18n = \frac{X[M+18n]}{100}$ where, n = number of water molecules, X= % loss from TGA and M = molecular weight of substance, is 5. From elemental and thermal analysis, the proposed formula of the complex is $Cs_5[PMo_{11}O_{39}Fe(H_2O)].5H_2O$.

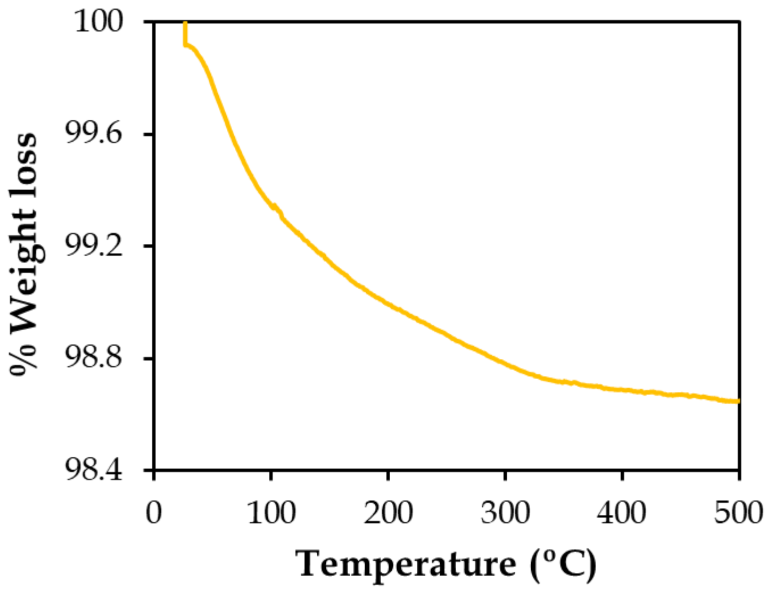

Figure 2. TGA curve of $PMo_{11}Fe$

The FT-IR spectra of PMo_{12}, PMo_{11}, and synthesized $PMo_{11}Fe$ are showed in figure 3. The FT-IR spectrum of PMo_{12} showed the characteristic stretching vibration bands at 1060 cm^{-1}, 965 cm^{-1}, 870 cm^{-1} and 790 cm^{-1} corresponding to v_s P-O_a, v_{as} Mo=O_t and v_{as} Mo-O_b-Mo and v_{as} Mo-O_c-Mo stretching vibration respectively [4, 28]. The FT-IR spectra of PMo_{11} showed characteristic splitting of P-O stretching bands at 1064 and 1045 cm^{-1} which indicate the formation of a lacuna by removing one Mo=O_t unit [4]. Also, it shows all other characteristic bands at 871 cm^{-1} corresponding to v_{as} Mo-O_b-Mo stretching and 791 cm^{-1} corresponding to vas Mo-O_c-Mo stretching vibrations. Similarly, the FT-IR spectra of $PMo_{11}Fe$ showed splitting in the P-O band at 1070, and 1041 cm^{-1} and other bands at 964 cm^{-1} (Mo=O_t), 873 cm^{-1} (Mo-O_b-Mo), and 783 cm^{-1} (Mo-O_c-Mo) respectively. The observed slight shift may be due to the distortion introduced by Fe on replacing Mo=O_t. Also, it shows one additional band at 516 cm^{-1} for Fe-O stretching frequency. Obtained results are in good agreement with reported ones [13-17].

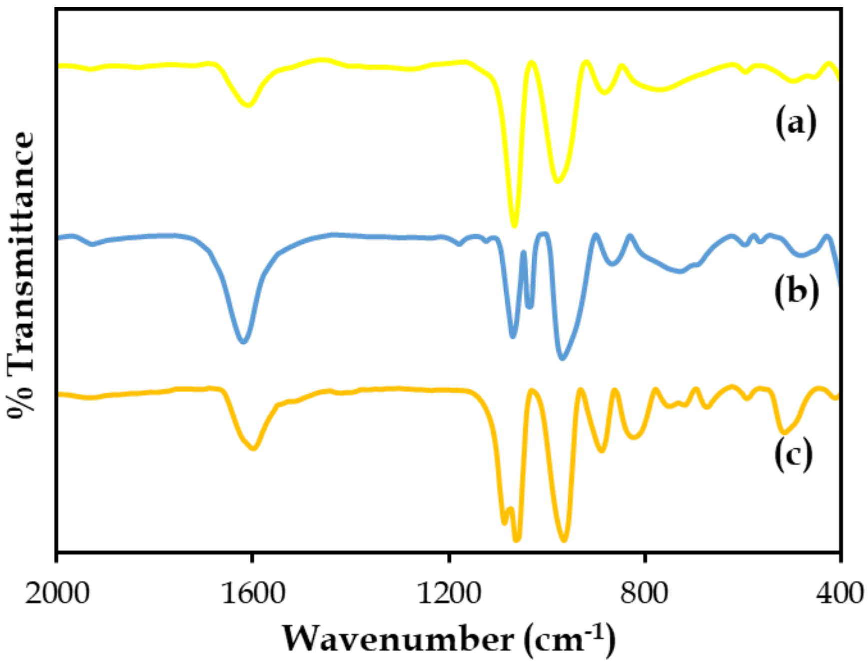

Figure 3. FT-IR spectra of (a) PMo_{12}, (b) PMo_{11}, and (c) $PMo_{11}Fe$

Table 1. Raman data of PMo_{12}, PMo_{11} and $PMo_{11}Fe$

Catalyst	$Mo{=}O_t$	$Mo\text{-}O_b\text{-}Mo$	$Mo\text{-}O_c\text{-}Mo$	$Mo\text{-}O_a$	$O_a\text{-}P\text{-}O_a$
PMo_{12}	v_s1005, v_{as} 987	v_{as} 916	v_{as} 620	v_{as} 251	-
PMo_{11}	v_s 947, v_{as} 932	v_{as} 891	v_{as} 550	v_{as} 217	v_{as} 355
$PMo_{11}Fe$	v_s 947, v_{as} 928	v_{as} 904	v_{as} 603	v_{as} 223	v_{as} 367

Raman spectra of PMo_{12}, PMo_{11} and $PMo_{11}Fe$ shown in figure 4 and Table 1. Where PMo_{12} (Table 1 and Figure 4b) shows stretching vibrations at 1005, 987, 916, 620 and 251 cm^{-1} corresponding to v_s $Mo{=}O_t$, v_{as} $Mo{=}O_t$, v_{as} $Mo\text{-}O_b\text{-}Mo$, v_{as} $Mo\text{-}O_c\text{-}Mo$ and v_{as} $Mo\text{-}O_a$ respectively. PMo_{11} shows characteristic bands at 947 cm^{-1} (v_s $Mo\text{-}O_t$), 932 cm^{-1} (v_{as} $Mo\text{-}O_t$), 891 cm^{-1} and 550 cm^{-1} (v_{as} $Mo\text{-}O_b\text{-}Mo$), 355 cm^{-1} (v_{as} $O_a\text{-}P\text{-}O_a$) and 217 cm^{-1} (v_s ($Mo\text{-}O_a$) respectively [29, 30]. Similarly, $PMo_{11}Fe$ (Figure 4b) show intense bands at 947 and a shoulder at 928 cm^{-1} due to the symmetric (v_s) and asymmetric (v_{as}) of $Mo{=}O_t$ respectively, sharp and broad bands at 904 and 603 cm^{-1} corresponding to v_{as} $Mo\text{-}O_b\text{-}Mo$, and band at 223 cm^{-1} corresponding to v_{as} $Mo\text{-}O_a$ stretching vibration, similar to PMo_{11}. Bands observed at 367 cm^{-1} corresponding to v_{as} $O_a\text{-}P\text{-}O_a$ (central tetrahedral PO_4) stretching indicates that the Keggin unit remains intact. However, the observed slight shifting for $PMo_{11}Fe$ may be due to the insertion of Fe into lacuna by removing one Mo.

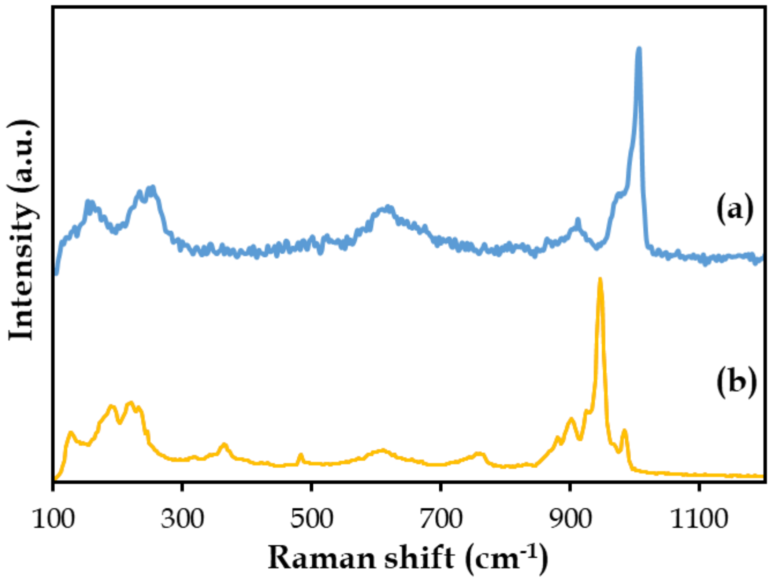

Figure 4. Raman spectra of (a) PMo_{12}, and (b) $PMo_{11}Fe$

^{31}P MAS NMR of PMo_{12} and $PMo_{11}Fe$ were carried out to understand the chemical environment around the phosphorus after insertion of Fe in to lacuna and purity of the synthesized catalyst. ^{31}P MAS NMR of PMo_{12} show (Figure 5) intense peak at -3.815 ppm which is in good agreement with reported one [14]. Whereas ^{31}P MAS NMR of $PMo_{11}Fe$ was (Figure 5) found to be silent due to insertion of Fe into the lacuna and formation of paramagnetic species (P-O-Fe^{3+}) [14, 31].

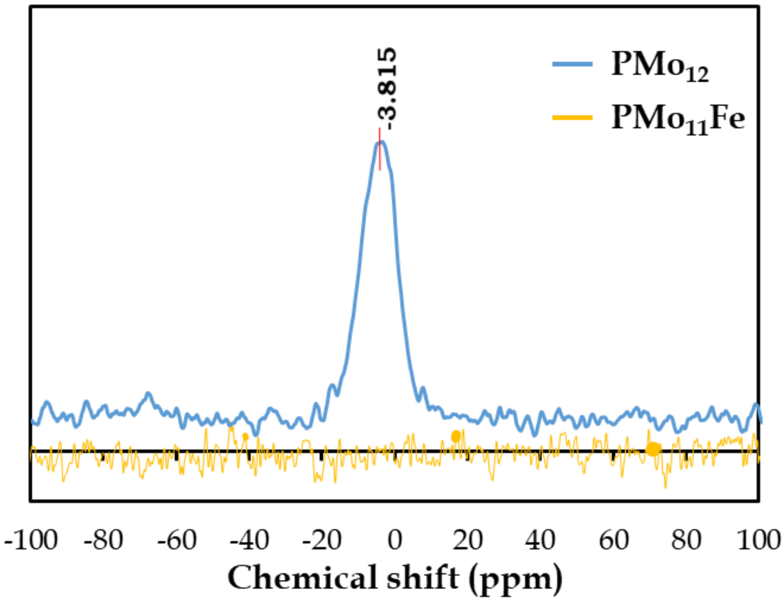

Figure 5. ^{31}P MAS NMR of (a) PMo_{12}, and (b) $PMo_{11}Fe$

The full range (5000–2500 G) X-band liquid nitrogen temperature ESR spectrum for $PMo_{11}Fe$ is presented in figure 6. $PMo_{11}Fe$ gives a single hyperfine spectrum with an isotropic signal, at g=4.3, assigned to Fe(III) with distorted octahedral geometry and it integrated (incorporated) with phosphomolybdate in high-spine (3+ state) [14]. The spin state of Fe(III) was confirmed by magnetic moment which was found to be 5.67 μ_B, and is in good agreement with theoretically calculated value and this also confirms that Fe in high spine state [31].

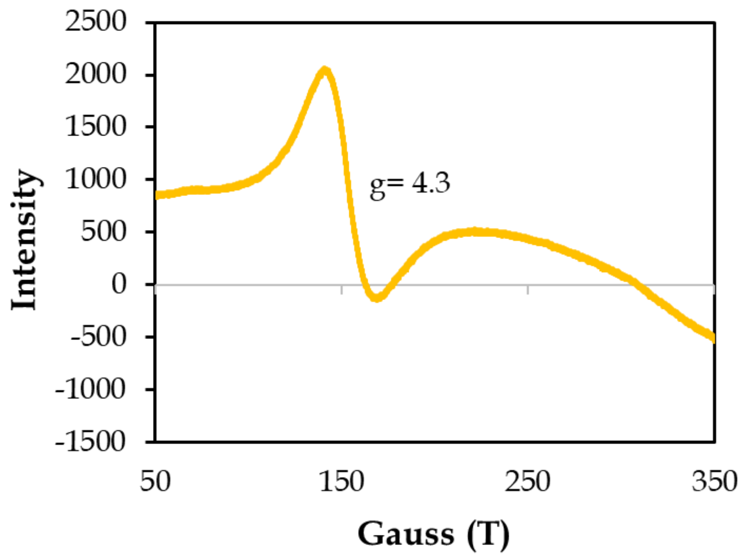

Figure 6. ESR spectra of $PMo_{11}Fe$

The chemical state of the PMo_{12} and $PMo_{11}Fe$ was investigated by X-ray photochemical spectroscopy (XPS). The XPS of PMo_{12} was well reported and it shows two significant binding energy peaks at 233.4 and 236.5 eV, which corresponds to $3d_{5/2}$ and $3d_{3/2}$ energy levels respectively and the peak at 134.2 eV attributes to 2P energy level of P [32-34]. The XPS of $PMo_{11}Fe$ (Figure 7) show intense peaks at binding energy level for Mo^{6+} as two doublets were observed; i) at 233.6 and 235.9 eV corresponding to $3d_{5/2}$ and $3d_{3/2}$ energy level ii) at 397, and 416 eV respectively for $3p_{3/2}$ and $3p_{1/2}$ energy level [35, 36]. The intense binding energy peak at 724 eV corresponding $Fe2p_{1/2}$ energy level, conforming the presence of Fe^{3+} [35, 36]. The low intense peak at 134.5 eV corresponding to 2p energy level of P. The obtained result indicates that there was no significant changes in the binding energy of Mo and P, which confirms that only one MoO unit has been replaced by iron in $PMo_{11}Fe$. Two additional high intense peaks at 532 eV and 724 eV are attributed to O1s and $Cs3d_{5/2}$, respectively [37, 38]. All found values are in good agreement with the reported one, confirming the presence of Fe and Mo in 3+ and 6+ states respectively in the synthesized complex.

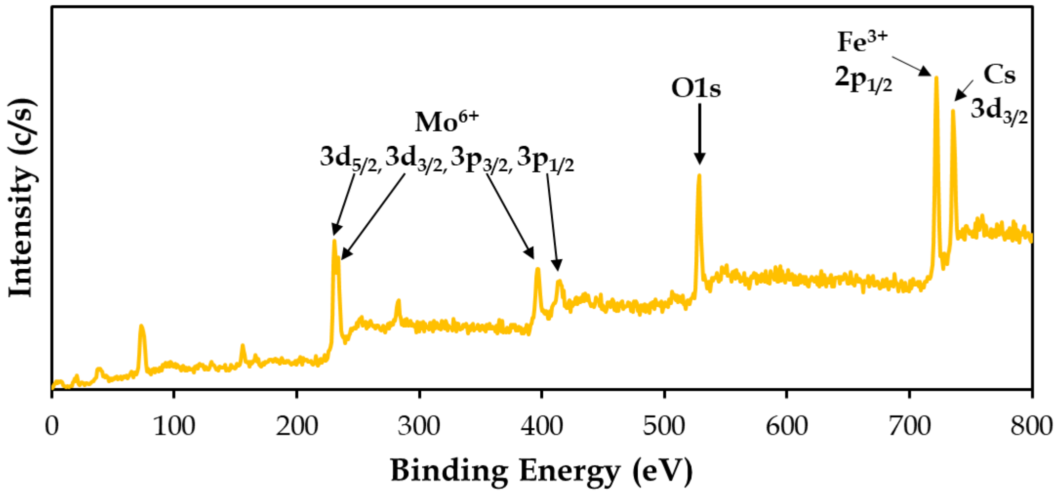

Figure 7. XPS of $PMo_{11}Fe$

The Powder XRD patterns of PMo_{12} and $PMo_{11}Fe$ are presented in figure 8. The XRD patterns of PMo_{12} (Figure 8a) showed all characteristic peaks in the range of 15° to 35° of 2θ [14]. A distinct shift in 2θ value of PMo_{11} (Figure 8b) from 25-35° is observed due to the formation of lacuna by removing one Mo=O unit. Similarly, the $PMo_{11}Fe$ XRD pattern (Figure 8b) shows all the characteristic peaks of Keggin unit, with slight shift peaks at 18.34°, 23.88°, 27° and 30.28° due to Fe incorporation with PMo_{11} [14, 17]**.** The above studies show that Keggin unit remains preserved even after Fe in the corporation.

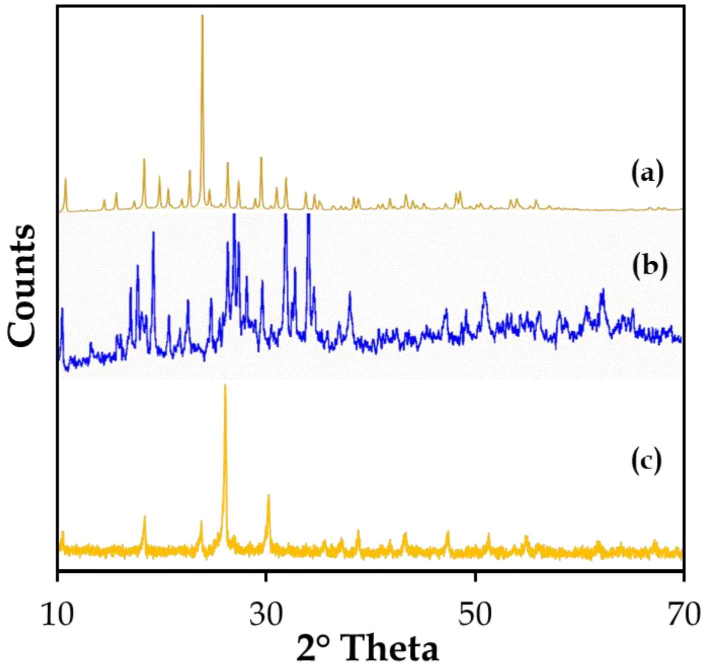

Figure 8. Powder XRD spectra of (a) PMo_{12}, (b) PMo_{11} and (b) $PMo_{11}Fe$

Therefore, FT-IR, Raman, powder XRD confirms the incorporation of iron into lacuna by replacing one MoO unit while XPS and ESR spectroscopy confirms the presence of Fe in a 3+ state with high spin and paramagnetic in nature.

Catalytic activity

Styrene hydrogention in aqueous medium:

The catalytic activity of $PMo_{11}Fe$ was evaluated for styrene hydrogenation (Scheme 2). Effect of various reaction parameters such as substrate-catalyst ratio, solvent, time, temperature, and hydrogen pressure were studied to obtain maximum conversion.

Table 2. Effect of solvent

Solvent	Amount (mL)	% conversion
H_2O	50	70
MeOH	50	89
EtOH	50	99
CH_3CN	50	20
MeOH : H_2O	20 : 30	64
EtOH : H_2O	20 : 30	90
CH_3CN : H_2O	20 : 30	54

Reaction conditions: catalyst (25 mg), styrene (10 mmol), H_2 Pressure (5 bar), solvent (50 ml), temperature (30 °C) and time (3 h).

As our main objective is to use environmentally benign solvents for the reaction, in the present study we have screened H_2O, MeOH, EtOH and CH_3CN as solvents and obtained results are shown in table 2. MeOH and EtOH showed high %conversion (89% and 99% respectively), which may be due to their reducing nature as compared to H_2O (70%) and CH_3CN (20%), because of their oxidizing nature. Reactions were also carried out using binary (aqueous medium) solvent systems such as MeOH: H_2O (1:1.5) and EtOH: H_2O (1:1.5), and a decrease in conversion as compared to neat solvent was observed. This may be due to the dilution effect which decreases their reducing nature. Interestingly, CH_3CN: H_2O resulted in the rise of conversion from 20 to 54% as the addition of water decreased, the amount of CH_3CN in the system. Also, the dispersion of styrene in MeOH, EtOH, H_2O and CH_3CN is different, which can lead to the diffusion problem and then affect the styrene conversion. Based on these results, the reaction was optimized using EtOH: H_2O solvent and the results are showed in table 3. Amongst, 1.5: 1 ratio of EtOH: H_2O gave optimum 99% conversion.

Table 3. Effect of EtOH: H_2O ratio

Solvent	%	%
C_2H_5OH : H_2O (mL)	Conversion	Selectivity
50 : 00	99	100
30 : 20	99	100
25 : 25	91	100
20 : 30	90	100
00 : 50	70	100

Reaction conditions: Catalyst (25 mg), styrene (10 mmol), H_2 Pressure (5 bar), temperature (30 °C) and time (3 h).

The amount of catalyst was optimized by varying from 25-5 mg, keeping all other parameters constant to obtain maximum conversion (Table 4). It is very interesting to note that there was no change in %conversion on lowering the catalyst amount up to 5 mg, however, from 25 -5 mg, TON number increased substantially from 1005 to 5031 from 25-5 mg indicating that 5 mg of the catalyst is active enough to achieve 99% conversion with single selectivity of ethylbenzene.

Table 4. Effect of catalyst amount

Catalyst Amount (mg)	% Conversion	% Selectivity	TON
25	99	100	1005
20	99	100	1256
15	99	100	1675
10	99	100	2513
5	99	100	5031

Reaction conditions: Styrene (10 mmol), H_2 Pressure (5 bar), EtOH: H_2O (30: 20 mL), temperature (30 °C) and time (3 h).

The obtained results (Table 4) may be due to the problem of inappropriate stirring of the reaction mass, observed by slurry formation [39] and there is possibility that the reaction may be prone to mass transfer limitations. Hence the reaction was carried out by varying mole of styrene and keeping the catalyst amount constant (Table 5).

Table 5. Effect of catalyst to styrene ratio

Styrene (mmol)	% Conversion	% Selectivity	TON
10	99	100	5031
15	83	100	6326
20	69	100	7012
25	49	100	6224
50	13	100	3302

Reaction conditions: Catalyst (5 mg), H_2 Pressure (5 bar), EtOH: H_2O (30: 20 mL), temperature (30 °C) and time (3 h)

As seen from the table 5, % conversion has decreased with increasing mole of styrene which confirms that the reaction rate is proportional to concentration of styrene and there is no mass transfer [40]. This is further confirmed by varying catalyst amount and by keeping moles of styrene constant, as shown in table 6. It was observed that % conversion and TON number increased with the increase in catalyst amount. From both table 5 and 6, reaction rate is governed by truly chemical step. Based on this result, 5mg catalyst was selected for 10 mmol of styrene for further optimization of other parameters.

Table 6. Effect of catalyst amount

Catalyst Amount (mg)	% Conversion	% Selectivity	TON
5	13	100	3303
10	25	100	3174
15	44	100	3723
20	63	100	3998
25	81	100	4113

Reaction conditions: Styrene (50 mmol), H_2 Pressure (5 bar), EtOH: H_2O (30: 20 mL), temperature (30 °C) and time (3 h)

Influence of hydrogen pressure on the reaction was screened from 3-5 bar (Figure 9a). The obtained results show that with increase in pressure, rate of % conversion was also increased from 54 to 99% linearly. Hence, the reaction is first order with respect to H_2 pressure which is in good agreement with reported one [41]. The optimum 99 % was achieved at 5 bar of H_2 pressure and it is used as an optimized reaction pressure for further study.

The effect of temperature on the reaction was also evaluated from 30-50 ^{0}C with an interval of 10 °C and obtained results are shown in figure 9b. No increase in conversion with temperature was found and hence 30 °C temperature was optimized.

Finally, reaction time was optimized by varying the reaction time from 1 to 3 h (Figure 9c) and keeping all other parameters constant to obtain maximum conversion. The obtained result show (Figure 9c) that with increasing time up to 3h, the % conversion was also increased, which is in good agreement with well-known fact that with increase in time, increase in formation of reactive intermediates from reactants which is further converted into products. The maximum conversion (99%) was obtained in 3h. Therefore, 3 h was optimized for the reaction.

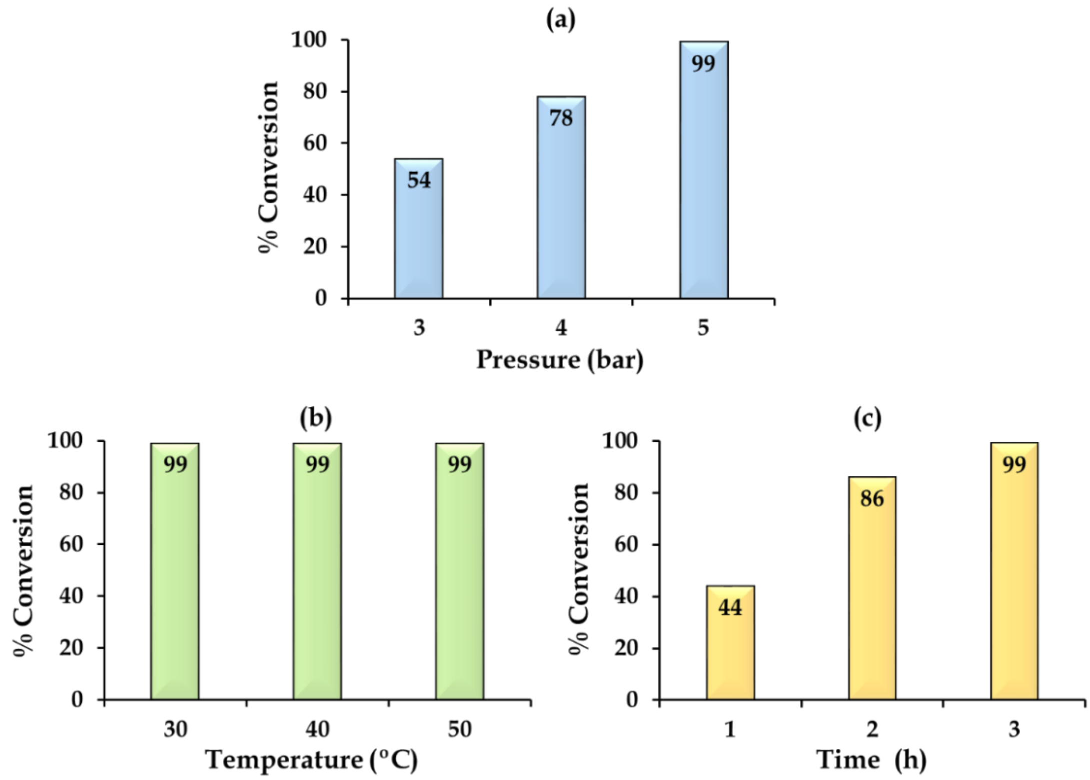

Figure 9. Optimization of reaction parameter for aqueous medium styrene hydrogenation. Reaction conditions: (a) Effect of pressure- catalyst (5 mg), styrene (10 mmol), EtOH: H_2O (30: 20 mL), temperature (30 °C) and time (3 h); (b) Effect of temperature- catalyst (5 mg), styrene (10 mmol), EtOH: H_2O (30: 20 mL), H_2 Pressure (5 bar) and time (3 h); (c) Effect of time- catalyst (5 mg), styrene (10 mmol), EtOH: H2O (30: 20 mL), H_2 Pressure (5 bar) and temperature (30 °C)

The optimized conditions for maximum, 99% conversion are: catalyst (5 mg), active amount of Fe (0.02 mol%), styrene (10 mmol), substrate /catalyst ratio (5081), EtOH: H_2O (30:20 mL), H_2 pressure (5 bar), time (3 h), temperature (30 °C), TON (5031).

The gas chromatograph of optimized conditions for aqueous medium is shown below in figure 10.

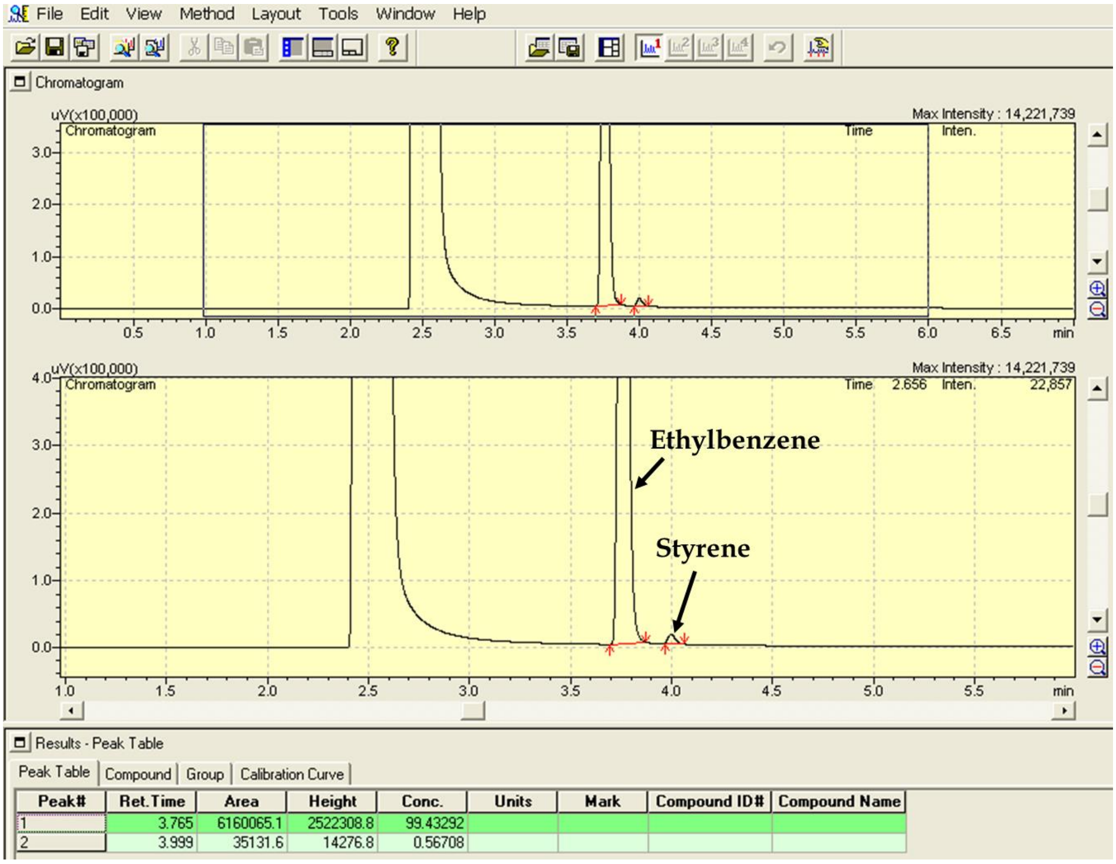

Figure 10. Gas chromatograph of styrene hydrogenation in aqueous medium

Styrene hydrogention in neat water

In an aqueous medium, the solvent study shows that in neat water 70% conversion was obtained, which is very interesting as so far iron based catalyst gets deactivated in the presence of neat water in the hydrogenation reaction. Therefore, it was thought to carry out a detailed study for styrene hydrogenation. Various parameters such as substrate to catalyst ratio, H_2 pressure, time and temperature have been studied to achieve maximum conversion.

The amount of catalyst was screened from 10-25 mg to achieve maximum conversion as shown in figure 11a. Obtained results show that conversion is increased with an increase in the amount of the catalyst from 10-25 mg and then it becomes almost constant It is observed that the TON number decreases with an increase in the amount of catalyst due to the increase in number of active sites, responsible for blocking. Looking at the maximum activity, the catalyst amount was optimized to 25 mg.

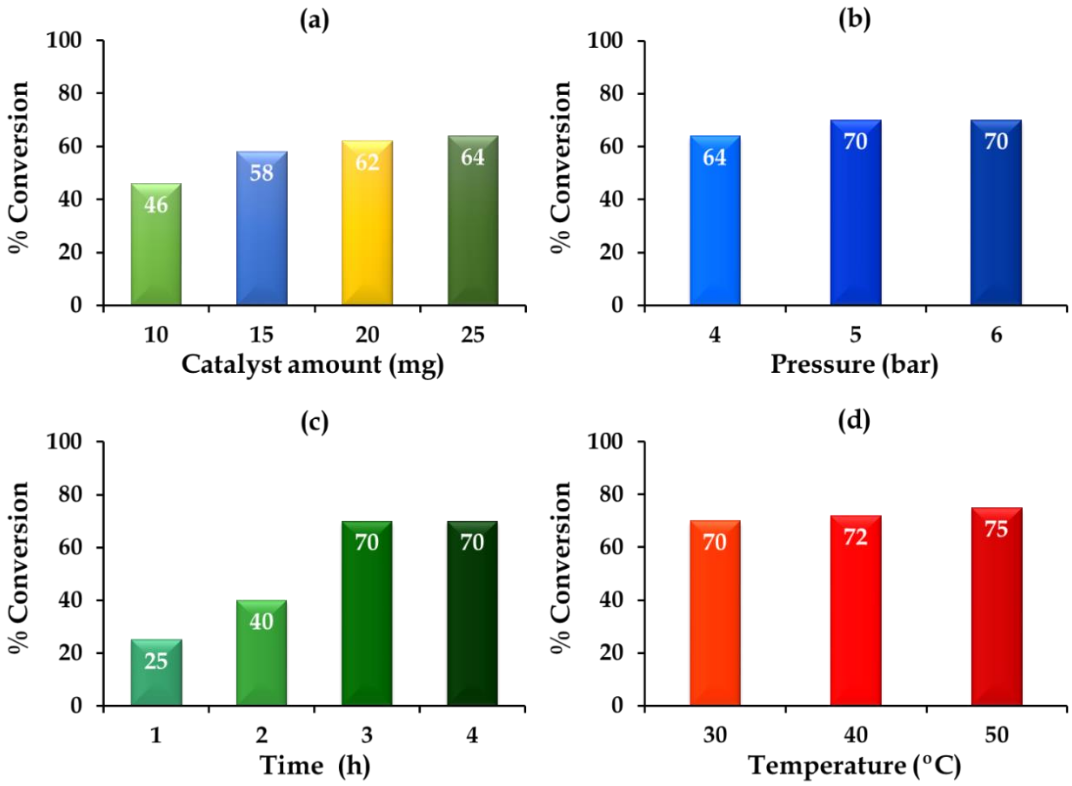

Figure 11. Optimization of reaction parameter for neat H_2O styrene hydrogenation. Reaction conditions: (a) Effect of catalyst amount- styrene (10 mmol), H_2 Pressure (5 bar), H_2O (50 mL), temperature (30 °C) and time (3 h); (b) Effect of pressure- cataalyst (25 mg), styrene (10 mmol), H_2O (50 mL), temperature (30 °C) and time (3 h); (c) Effect of temperature- cataalyst (25 mg), styrene (10 mmol), H_2O (50 mL), H_2 Pressure (5 bar), and time (3 h); (d) Effect of time- cataalyst (25 mg), styrene (10 mmol), H_2O (50 mL), H_2 Pressure (5 bar) and temperature (30 °C).

Other parameters such as H_2 pressure, time and temperature were also varied (Figure 11b-d) to achieve the maximum activity.

The optimized condition for maximum 70% conversion are: catalyst amount (25 mg), active amount of Fe (0.1 mol%), styrene (10 mmol), substrate /catalyst ratio (1015), H_2 pressure (5 bar), time (3 h), temperature (30 °C), water (50 mL) and TON (710).

The gas chromatograph of optimized reaction conditions for neat H_2O is shown in figure 12.

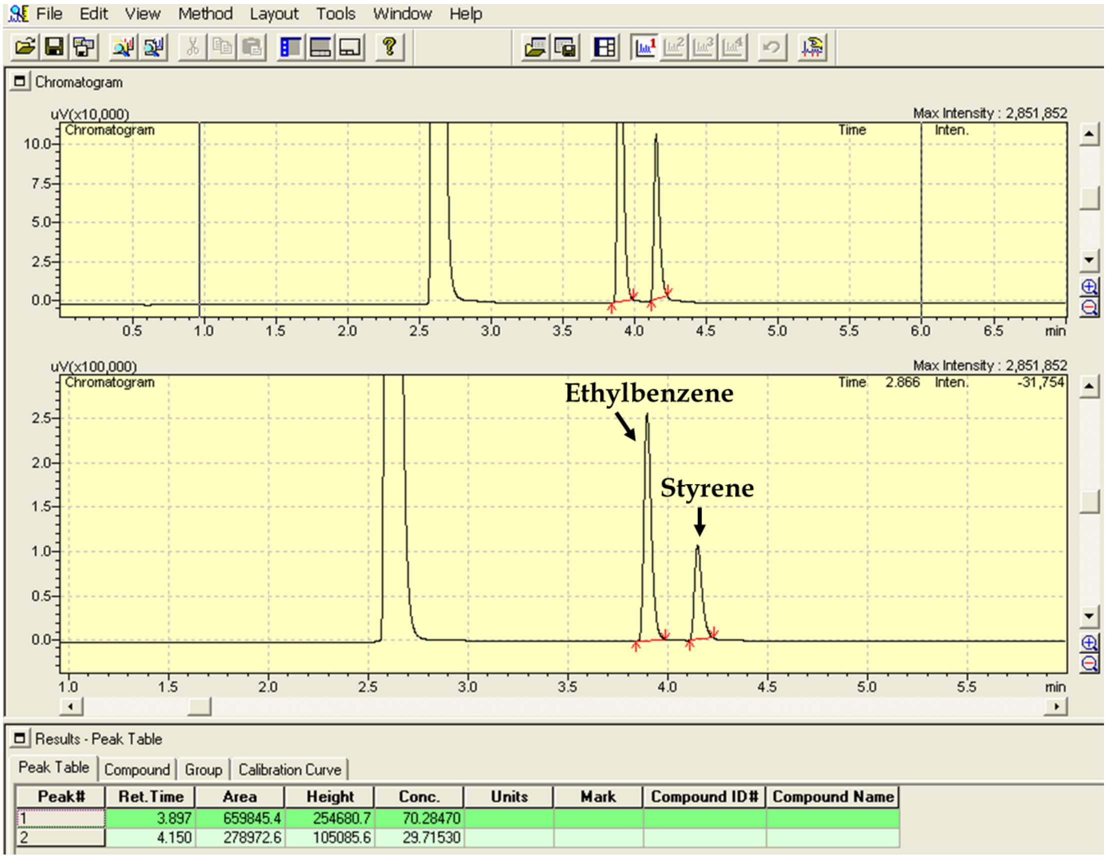

Figure 12. Gas chromatograph of styrene hydrogenation in neat water

Table 7. Effect of solvent on % conversion

Catalyst	Catalyst amount	Solvent	% Conversion	TON
$PMo_{11}Fe$	5	[a]EtOH: H_2O (aqueous medium)	99	5013
	25	[b]Neat H_2O	70	710

[a]Reaction conditions for aqueous medium: Catalyst (5 mg; Fe: 0.02 mol%), styrene (10 mmol), H_2 pressure (5 bar), time (3 h), temperature (30 °C), EtOH: H_2O (30: 20 mL).

[b]Reaction conditions for neat water: Catalyst (25 mg; Fe: 0.1 mol%), styrene (10 mmol), H_2 pressure (5 bar), time (3 h), temperature (30 °C), H_2O (50 mL).

From the table 7, it is interesting to note that in both solvent systmes (aqueous medime and neat H_2O) good % Conversion was achived and therefore chemist can select either one depending on his/her requirement. In the present study, we have selected an aqueous medium from the viewpoint of minimum used amount of the catalyst (5 mg), % conversion (99%) and higher TON (5013).

Control experiments

To investigate the role of individual components, a control experiment was performed without H_2, without catalyst, using $Fe(NO_3)_3$ with the active amount of Fe and with the active amount of PMo_{11} under optimized reaction conditions and results are shown in table 8. There was no conversion found, when the reaction was performed without H_2 pressure and without catalyst under identical reaction conditions, which indicates that H_2 and catalyst both are essential for the reaction progress. Both $Fe(NO_3)_3$ and PMo_{11} gave low conversion in an aqueous medium and water medium. From these results, it can be confirmed that Fe of $PMo_{11}Fe$ is responsible for the maximum conversion.

Table 8. Control experiments

Catalyst	% [a]Conversion	% [b]Conversion
Without H_2	-	-
Without catalyst	-	-
$Fe(NO_3)_3$	36	28
PMo_{11}	10	6
$PMo_{11}Fe$	99	70

[a]Reaction conditions for aqueous medium: Catalyst (5 mg; Fe: 0.02 mol%), styrene (10 mmol), H_2 pressure (5 bar), time (3 h), temperature (30 °C), EtOH: H_2O (30: 20 mL).
[b]Reaction conditions for neat water: Catalyst (25 mg; Fe: 0.1 mol%), styrene (10 mmol), H_2 pressure (5 bar), time (3 h), temperature (30 °C), H_2O (50 mL).

Hot filtration and heterogeneity test

As the catalyst is heterogeneous, the leaching of Fe from lacuna was investigated by hot filteration test. The test was carried out by simply centrifuging the catalyst between the reactions in both cases. In both the reactions, the first reaction was carried out for 1h, the catalyst was removed by centrifugation, and then the resulting filtrate was allowed to react up to 3 h. After completion of the reaction, the organic phase was extracted by dichloromethane and analyzed by Gas chromatogram. In both the cases, the obtained results (Table 9) show that after removal of the catalyst, there was no significant change in % conversion, which display that there was no leaching of Fe during both reactions. This study indicates that catalyst is truly heterogeneous to be recycled and reused.

Table 9. Hot filtration test

Catalyst	% [a]Conversion	% [b]Conversion
$PMo_{11}Fe$	44 (after 1 hour)	26 (after 1 hour)
	45 (after 3 hour)	27 (after 3 hour)

[a]Reaction conditions for aqueous medium: Catalyst (5 mg; Fe: 0.02 mol%), styrene (10 mmol), H_2 pressure (5 bar), time (3 h), temperature (30 °C), EtOH: H_2O (30: 20 mL).
[b]Reaction conditions for neat water: Catalyst (5 mg; Fe: 0.1 mol%), styrene (10 mmol), H_2 pressure (5 bar), time (3 h), temperature (30 °C), water (50 mL).

Regeneration and recycling studies

Sustainability is the key issue for any catalytic process and the same recovery and reusability tests were performed for the present catalyst. After completion of the reaction, the catalyst was regenerated by simple centrifugation and the organic phase was extracted by dichloromethane. The regenerated catalyst was washed with dichloromethane followed by subsequent washes with distilled water and finally dried in air to reuse for the next catalytic run under optimized conditions. In both the cases (in aqueous and net water medium) obtained results show (Table 10) that there is no significant change in conversion up to two-cycle. This indicates that the catalyst is stable and can be reused essential for the progress of a reaction.

Table 10. Recycling studies

Catalyst	a/b% Conversion	a/b TON
$PMo_{11}Fe$	99/70	5031/710
Recycle – 1	99/69	5031/709
Recycle – 2	98/69	5031/709

[a]Reaction conditions for aqueous medium: Catalyst (5 mg; Fe: 0.02 mol%), styrene (10 mmol), H_2 pressure (5 bar), time (3 h), temperature (30 °C), EtOH: H_2O (30: 20 mL).
[b]Reaction conditions for net water: Catalyst (5 mg; Fe: 0.1 mol%), styrene (10 mmol), H_2 pressure (5 bar), time (3 h), temperature (30 °C), water (50 mL).

Characterization of regenerated catalyst

The regenerated catalyst $PMo_{11}Pd$ was characterized by EDX, FT-IR, ESR and XPS analysis for the confirmation of the catalyst structure retention.

For regenerated $PMo_{11}Fe$, EDX values (Cs: 26.00%, P: 1.21%, Mo: 41.28%, Fe: 2.18%, O: 28.79%) and ICP values (P: 1.31%, Mo: 42.40%, Fe: 2.54%) are in good agreement with a fresh one, indicates that there was no leaching of Fe during the reaction. EDX mapping shows (Figure 13) the presence of Cs, P, Mo, Fe and O in the regenerated catalyst.

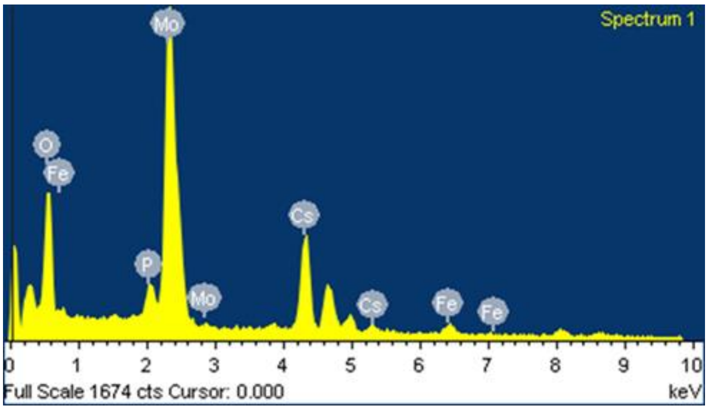

Figure 13. EDX mapping of regenerated -$PMo_{11}Fe$

The FT-IR spectrum of fresh and regenerated catalysts are shown in figure 14. An almost identical spectrum was found without any significant shift in the bands of regenerated $PMo_{11}Fe$ as compared to the $PMo_{11}Fe$, indicates that the structure of the catalyst remains unchanged even after regeneration. However, in terms of intensity, the spectrum is slightly different from the fresh one. This could be due to sticking of the substrates on the surface of the catalyst, although this may not be significant when the catalyst is reused.

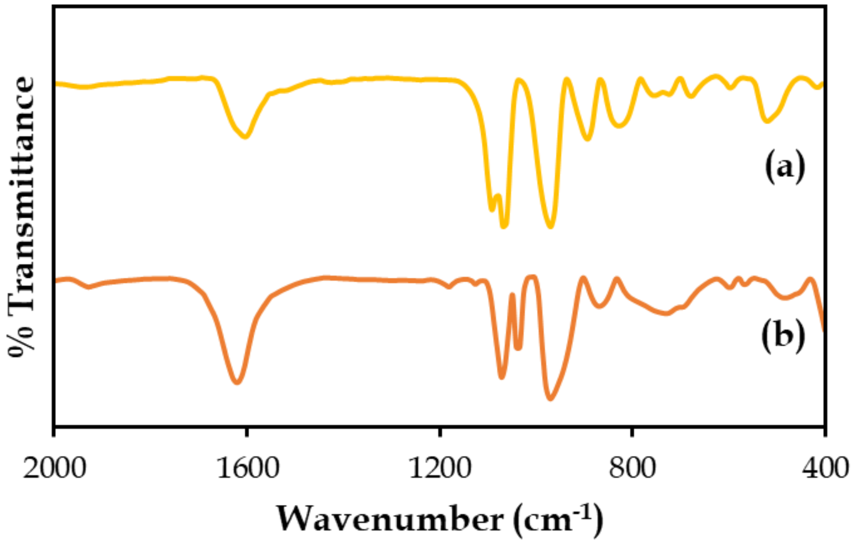

Figure 14. FT-IR of (a) Fresh $PMo_{11}Fe$ and (b) Regenerated $PMo_{11}Fe$

From figure 15, it is seen that ESR spectra of regenerated $PMo_{11}Fe$ give a single hyperfine spectrum with an isotropic signal, observed at g=4.3, which is identical with fresh catalyst, $PMo_{11}Fe$. The obtained result indicates that the catalyst remains intact even after regeneration.

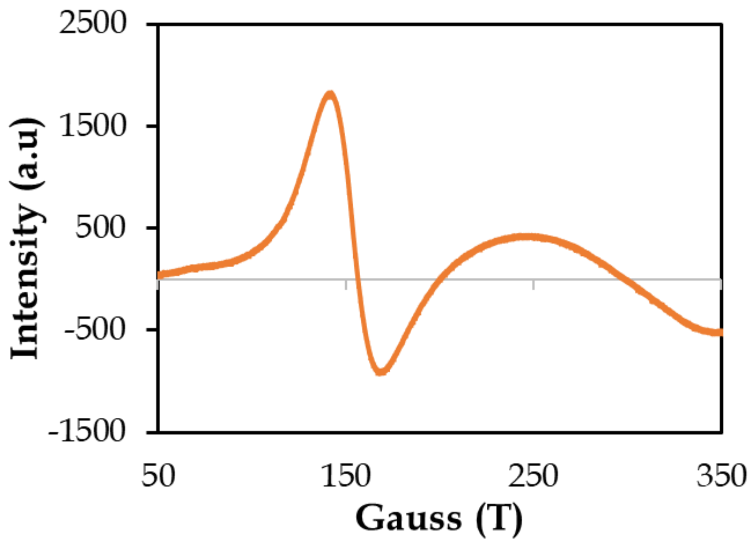

Figure 15. ESR spectra of Regenerated $PMo_{11}Fe$

The XPS of regenerated $PMo_{11}Fe$ is shown in figure 16. The obtained spectrum shows intense peaks at 234, 236, 397 and 416 eV which corresponds to 3d and 3p energy level of Mo(VI) and also shows the intense peak at 724 eV which corresponds to 2p energy level of Fe(III). The obtained spectrum is identical with the fresh one (Figure 7) indicating the sustainability of the catalyst.

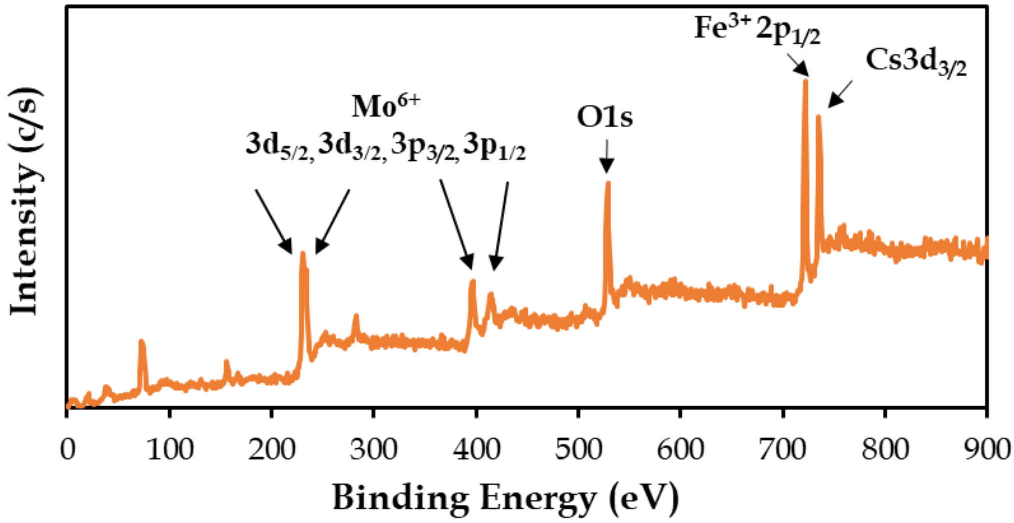

Figure 16. XPS of of Regenerated $PMo_{11}Fe$

Mechanistic investigation

Fe catalyzed styrene hydrogenation proceeds through two different possible mechanistic pathways: i) by chemisorption (by Fe(III) reduced to Fe (II)) and ii) by physisorption (by adsorption-desorption) [42, 43]. To know the mechanistic pathway with the present catalyst, control experiments, as well as the reaction, carried out under N_2 pressure and D_2O as solvent were also performed. i) Control experiments show (Table 8) that the Fe is the only active species and H_2 pressure is also essential for the progress of a reaction. ii) Reaction was carried out under N_2 instead of H_2 to confirm the necessity of H_2 and the role of water during the reaction. The obtained result (no conversion) shows (Figure 17a) that H_2 is also essential for reaction progress and water acts as a solvent. iii) Further, to confirm the role of water as solvent or proton transfer agent during the reaction, the reaction was carried out in D_2O instead of H_2O (Figure 17b).

The absence of the deuterated product in ^{1}H NMR (Figure 17c) indicates that the hydrogen was directly transferred from the H_2 gas rather than water.

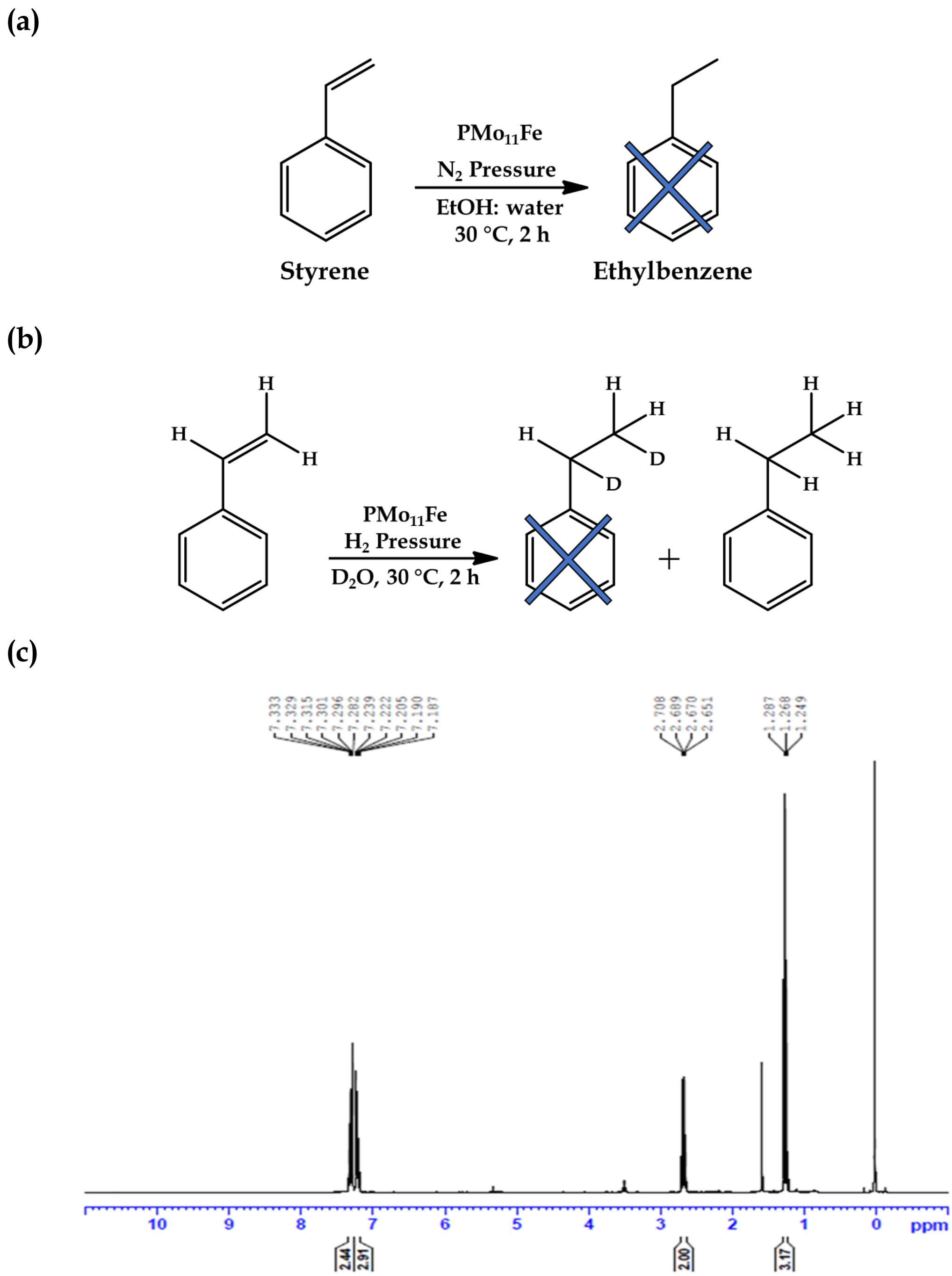

Figure 17. (a) reaction under N_2 pressure, (b) reaction in D_2O and (c) ^{1}H NMR of reaction carried out in D_2O

Further, to confirm any change in the oxidation state of Fe 3+ responsible for chemisorption, ESR spectra of the catalyst after quenching of reaction at 1 h, 1.5 h and 2 h were carried out. The ESR spectra of catalyst obatined after 1 h, 1.5 h and 2 h (Figure 18) are similar with that of the fresh one, which confirms that no chemisorption takes place and the reaction proceeds through physisorption pathway.

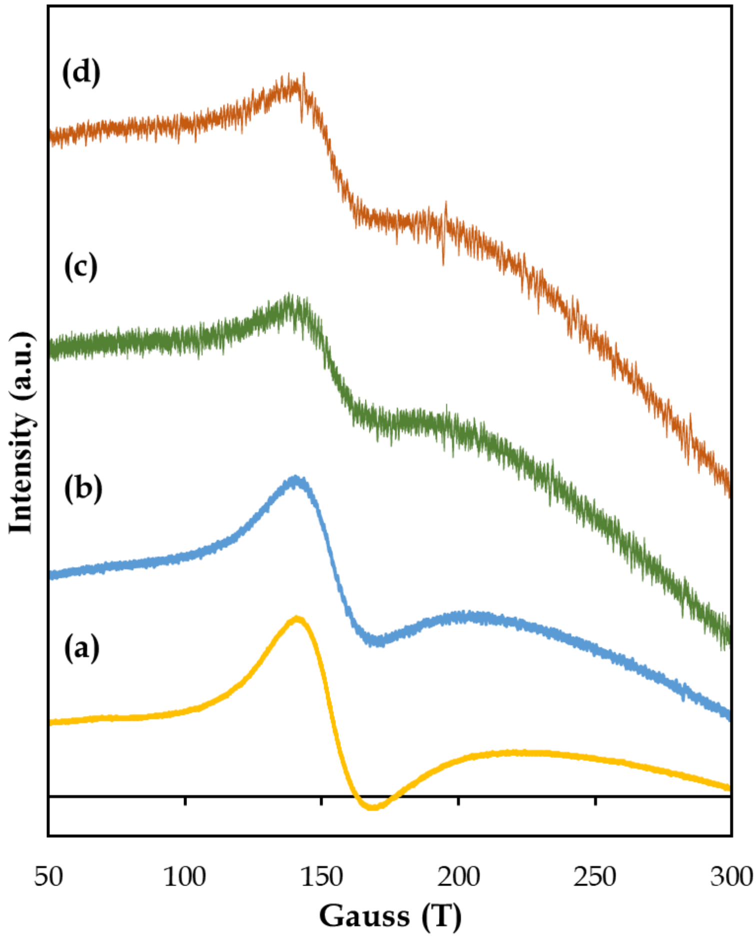

Figure 18. ESR spectra of (a) fresh catalyst, (b) after 1 h, (c) after 1.5 h and (d) after 2 h

From the above evidences, the possible adsorption-desorption mechanism of styrene hydrogenation is proposed in scheme 3, which is similar to the one as reported earlier by Corma group [42]. In this, first H_2 gets adsorbed on Fe-OH_2 (green colour) and Mo=O-H site followed by heterolytic cleavage. Styrene gets adsorbed on catalyst surface at hydroxyl assisted Mo=O-H site. After that, the generated Fe-H hydride was transferred to a double bond of styrene followed by the transfer of H^+ from Mo=O-H to form ethylbenzene. Finally, the resulting desired product, alkane (ethylbenzene) gets desorbed and the active site of the catalyst gets regenerated for further hydrogenation. We are expecting the same mechanism for an aqueous system (EtOH: H_2O).

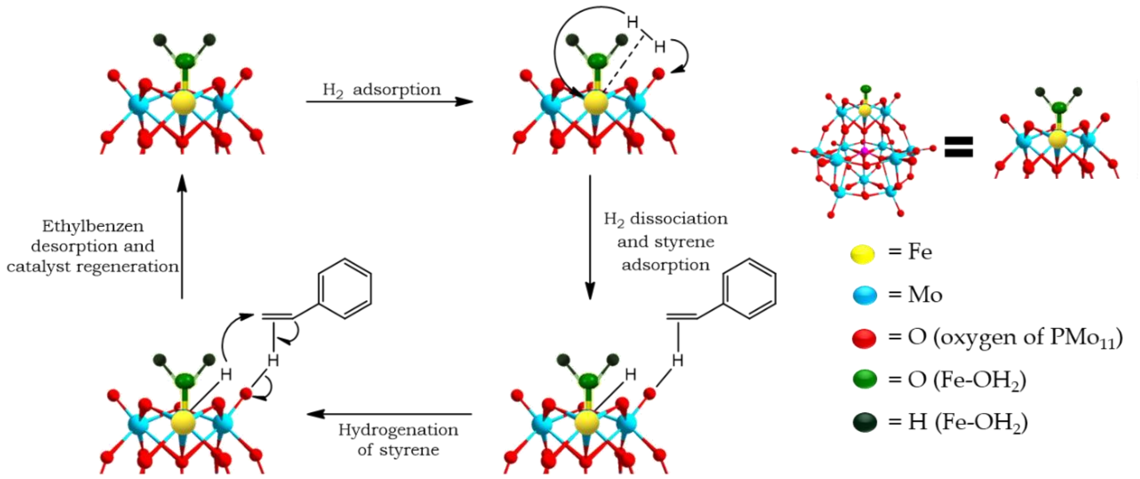

Scheme 3. Plausible mechanism of styrene hydrogenation.

Viability of the catalyst

To see the viability of the catalyst, hydrogenation of various substrates were carried out under optimized conditions and the obtained results are shown in table 11. The catalyst shows appreciable reactivity towards styrene derivatives with a good conversion rate. However, the observed low % conversion for the planar and non-planar cyclic alkene may be due to the difficulty to approach the catalytic active site during the reaction and could increase the conversion in harsh conditions. Whereas, tha catalyst was totally inactive for the levilinic acid hydrogenation under optimized condition because hydrogenation of carbonyl group (C=O) which present in levulinic acid requires harsh conditions.

Table 11. Substrate study

Substrate	Product	% conversion
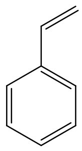	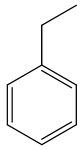	99
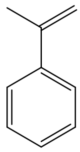	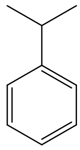	91
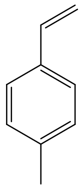	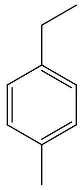	95
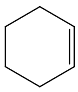	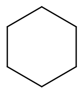	61
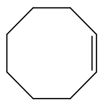	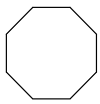	35
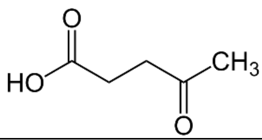	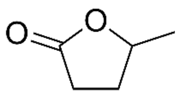	00

Reaction conditions for aqueous medium: Catalyst (5mg), styrene (10 mmol), H_2 pressure (5 bar), time (3 h), temperature (30 °C), EtOH: H_2O (30: 20 mL).

Comparison with reported catalyst

The efficacy of the present catalyst was compared with the reported system for styrene hydrogenation in terms of reaction conditions shown in table 12.

For styrene hydrogenation, Moores et al. [23] achieved 100% conversion at high temperature and very high H_2 pressure (40 bar) compared to the present system. Further, the same group reported 100% conversion using high temperature and high catalyst amount compared to the present system [44]. The hydrazine hydrated as a proton transfer agent was reported by Nadagouda et al. for 98% conversion using moderate condition with a high catalyst underwater medium [45]. Jones et al. achieved 100% conversion by using deuterated benzene as a solvent at 23 °C and 24 h [46]. Further, the calculated TON/ TOF also shows that the present catalyst is best amongst all the reported systems.

Table 12. Comparison of styrene hydrogenation with reported systems

Catalyst	Fe (mol %)	Solvent	Reducing agent	Time (h)	Temp. (°C)	% Conversion	TON/ TOF
Fe CSNPs [5]	5	ethanol	H_2 (40 bar)	24	80	100	20/ 0.83
FeNP@PS-PEG-NH_2 [30]	11.72	ethanol	H_2 (40 bar)	6	100	44	2/ 0.33
Fe@g-C_3N_4 [31]	4.47	water	$NH_2NH_2.H_2O$	8	-	98	22/ 2.75
$(PNHP^{iPr})Fe(H)_2(CO)$ [32]	5	deuterated benzene	H_2 (01 bar)	24	23	100	20/ 0.83
$PMo_{11}Fe$ (Present Work)	**0.02**	**ethanol: water**	**H_2 (05 bar)**	**3**	**30**	**99**	**5031/ 1684**

CONCLUSION

- **$Cs_5[PMo_{11}O_{39}Fe(H_2O)].5H_2O$** was synthesized by **one-pot** method and characterized by various **physicochemical techniques to** confirm the **Fe incorporation** into **lacuna** with retention of Keggin unit.
- The catalyst depicts the **high efficiency** towards styrene hydrogenation (**99 % conversion)** at room temperature (30 °C) in **aqueous medium** (EtOH: H_2O) as a green solvent.
- **Recycling and reusability** studies show that the catalyst is **sustainable** up to three catalytic cycles **without significant loss** in catalytic activity.
- **Substrate study** shows that the catalyst is **highly viable** towards different **types of substrates.**
- The **superiority** of the present catalyst lies in terms of **conversion, active amount of Fe (0.02 mol%), mild reaction conditions and TON/TOF (5081/1684)**.

REFERENCES

[1] S. T. Yamaguchi, S. Sumimoto, Y. Ichihashi, S. Nishiyama, S. Tsuruya, Ind. Eng. Chem. Res., 44, 1, (2005).

[2] A. Patel, S. Pathan, J. Coord. Chem., 65, 3122, (2012).

[3] S. Pathan, A. Patel, Appl. Catal. A: Gen., 459, 59, (2013).

[4] S. Pathan, A. Patel, Catal. Sci. Technol., 4, 648, (2014).

[5] P. Villabrille, G. Romanelli, P. Vázquez, C. Cáceres, Appl. Catal. A: Gen., 270, 101, (2004).

[6] Q. Huynh, Y. Schuurman, P. Delichere, S. Loridant, J. M. M. Millet, J. Catal., 261, 166, (2009).

[7] G. Chi, Y. Qi, J. Li, L. Wang, J. Hu, J. Inorg. Biochem., 193, 173, (2019).

[8] I. El Arrouji, A. Oulmekki, M. Taoufik, F. Lefebvre, J. Toyir, Mater. Today Proc., 51, 2015, (2022).

[9] J. Díaz, L. R. Pizzio, G. Pecchi, C. H. Campos, L. Azócar, R. Briones, R. Romero, A. Henríquez, E. M. Gaigneaux, D. Contreras, Catalysts, 12, 507, (2022).

[10] M. José da Silva, J. A. Vergara Torres, C. B. Vilanculo, RSC Adv., 12, 11796, (2022).

[11] J. Hu, R. C. Burns, J. Mol. Catal. A: Chem., 184, 451, (2002).

[12] R. Karcz, K. Pamin, J. Połtowicz, J. Haber, Catal. Lett., 132, 159, (2009).

[13] C. Knapp, T. Ui, K. Nagai, N. Mizuno, Catal. Today, 71, 111, (2001).

[14] N. Mizuno, J.-S. Min, A. Taguchi, Chem. Mater., 16, 2819, (2004).

[15] T. Mazari, C. R. Marchal, S. Hocine, N. Salhi, C. Rabia, J. Nat. Gas Chem., 18, 319, (2009).

[16] R. Xing, A. Zheng, F. Wang, L. Wang, Y. Yu, A. Jiang, Food Chem., 175, 292, (2015).

[17] M. Rabbani, Z. S. Seghatoleslami, R. Rahimi, J. Mol. Struct., 1146, 113, (2017).

[18] D. Hu, X. Song, H. Zhang, X. Chang, C. Zhao, M. Jia, Mol. Catal., 506, 111552, (2021).

[19] X. Chen, J. Wang, Y. Yu, H. Chen, X. Wu, S. Gao, Catal. Lett., 152, 3807, (2022).

[20] Y. Ghandour, C. McHiri, I. Mestiri, A. Y. A. Alzahrani, H. Nasri, J. Chem. Sci., 134, 78, (2022).

[21] A. Tian, H. Ni, Y. Tian, X. Ji, G. Liu, J. Ying, Inorg. Chem. Commun., 68, 50, (2016).

[22] M. A. Rezvani, M. Shaterian, F. Akbarzadeh, S. Khandan, Chem. Eng. J., 333, 537, (2018).

[23] R. Hudson, A. Rivière, C. M. Cirtiu, K. L. Luska, A. Moores, Chem. Comm., 48, 3360, (2012).

[24] A. A. Shesterkina, L. M. Kustov, A. A. Strekalova, V. B. Kazansky, Catal. Sci. Technol., 10, 3160, (2020).

[25] B. Husson, M. Ferrari, O. Herbinet, S. S. Ahmed, P.-A. Glaude, F. Battin-Leclerc, Proc. Combust. Inst., 34, 325, (2013).

[26] Z. Luo, S. Qin, S. Chen, Y. Hui, C. Zhao, Green Chem., 22, 1842, (2020).

[27] A. I. Vogel, J. Mendham, Vogel's Textbook of Quantitative Chemical Analysis, Pearson Education Asia, (2000).

[28] K. T. V. Rao, B. Haribabu, P. S. S. Prasad, N. Lingaiah, ChemCatChem, 4, 1173, (2012).

[29] N. Narkhede, A. Patel, S. Singh, Dalton Trans., 43, 2512, (2014).

[30] T. A. G. Duarte, I. C. M. S. Santos, M. M. Q. Simões, M. G. P. M. S. Neves, A. M. V. Cavaleiro, J. A. S. Cavaleiro, Catal. Lett., 144, 104, (2014).

[31] A. A. Zatsiupa, L. A. Bashkirov, I. O. Troyanchuk, G. S. Petrov, A. I. Galyas, L. S. Lobanovsky, S. V. Truhanov, J. Solid State Chem., 212, 147, (2014).

[32] M. Lei, Q. Gao, K. Zhou, P. Gogoi, J. Liu, J. Wang, H. Song, S. Wang, X. Liu, Sep. Purif. Technol., 257, 117933, (2021).

[33] B. Zhang, H. Asakura, J. Zhang, J. Zhang, S. De, N. Yan, Angew. Chem. Int. Ed., 55, 8319, (2016).

[34] B. Zhang, G. Sun, S. Ding, H. Asakura, J. Zhang, P. Sautet, N. Yan, J. Am. Chem. Soc., 141, 8185, (2019).

[35] C. Wan, B. M. Leonard, Chem. Mater., 27, 4281, (2015).

[36] D. Yu, W. Gao, S. Xing, L. Lian, H. Zhang, X. Wang, D. lou, RSC Adv., 9, 4884, (2019).

[37] A. Patel, A. Patel, Catal. Lett., 151, 803, (2021).

[38] W. T. Liu, S. C. Tsai, T. L. Tsai, C. P. Lee, C. H. Lee, J. Radioanal. Nucl. Chem., 314, 2237, (2017).

[39] C. Xiros, M. Janssen, R. Byström, B. T. Børresen, D. Cannella, H. Jørgensen, R. Koppram, C. Larsson, L. Olsson, A.-M. Tillman, S. Wännström, Biofuels, Bioproducts and Biorefining, 11, 15, (2017).

[40] G. C. Bond, Heterogeneous Catalysis: Principles and Applications, Clarendon Press, (1982).

[41] C. U. I. Odenbrand, S. T. Lundin, J. Chem. Technol. Biotechnol., 31, 660, (1981).

[42] M. Tejeda-Serrano, M. Mon, B. Ross, F. Gonell, J. Ferrando-Soria, A. Corma, A. Leyva-Pérez, D. Armentano, E. Pardo, J. Am. Chem. Soc., 140, 8827, (2018).

[43] M. Tejeda-Serrano, J. R. Cabrero-Antonino, V. Mainar-Ruiz, M. López-Haro, J. C. Hernández-Garrido, J. J. Calvino, A. Leyva-Pérez, A. Corma, ACS Catal., 7, 3721, (2017).

[44] R. Hudson, G. Hamasaka, T. Osako, Y. M. A. Yamada, C.-J. Li, Y. Uozumi, A. Moores, Green Chem., 15, 2141, (2013).

[45] R. B. N. Baig, S. Verma, R. S. Varma, M. N. Nadagouda, CS Sustain. Chem. Eng., 4, 1661, (2016).

[46] R. Xu, S. Chakraborty, S. M. Bellows, H. Yuan, T. R. Cundari, W. D. Jones, ACS Catal., 6, 2127, (2016).

CHAPTER 2

Iron exchanged phosphomolybdic acid supported on zirconia (Fe-PMo_{12}/ZrO_2): Synthesis, characterization and application for hydrogenation of cyclohexene

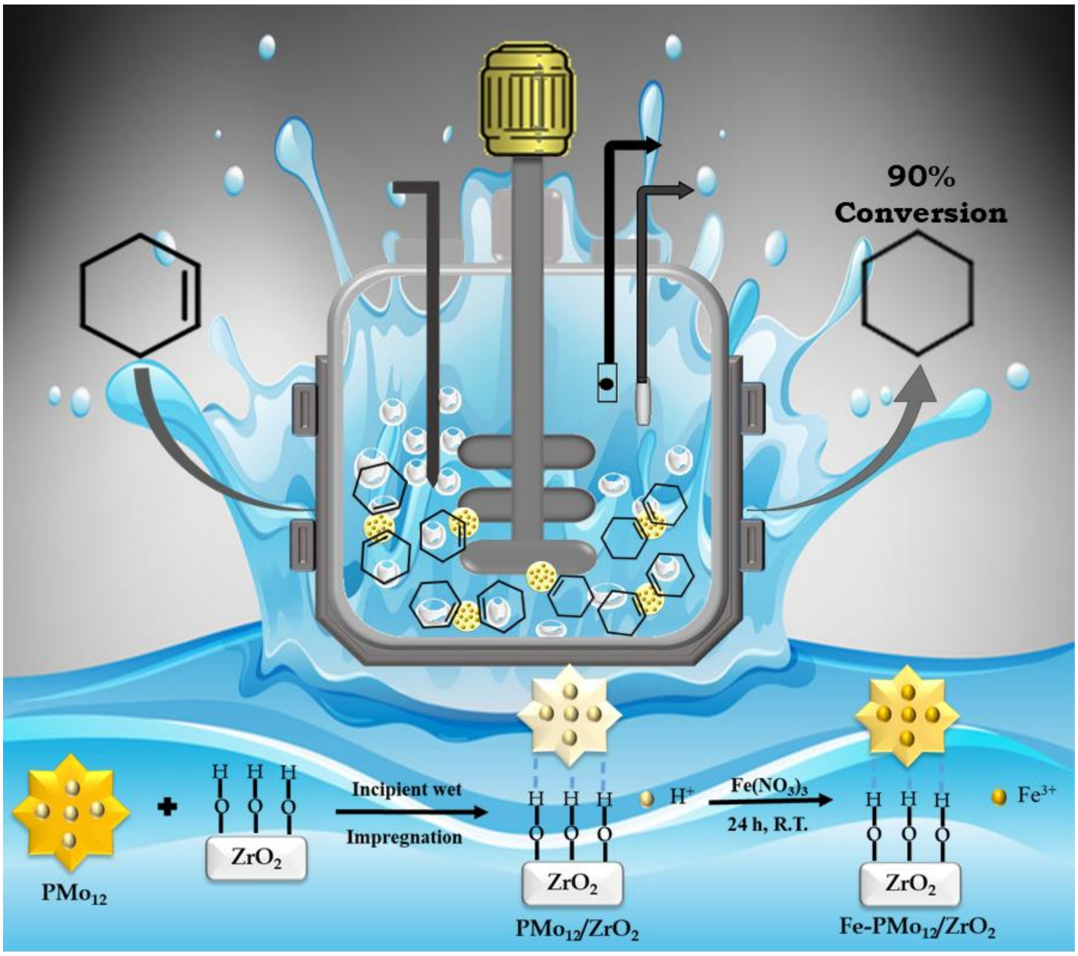

Catalysis Letters
https://doi.org/10.1007/s10562-021-03838-8

Fe Exchanged Supported Phosphomolybdic Acid: Synthesis, Characterization and Low Temperature Water Mediated Hydrogenation of Cyclohexene

Anjali Patel[1] · **Jay Patel**[1]

Received: 29 July 2021 / Accepted: 22 October 2021

Abstract
In this article, first time we are reporting two steps synthesis of Fe exchanged phosphomolybdic acid supported on zirconia (Fe-PMA/ZrO_2) by incipient wet impregnation and ion exchange method. The obtained material was well characterized by EDX mapping, ICP, FT-IR, Raman, ^{31}P MAS NMR, ESR, XPS and powder XRD. The catalytic evaluation was explored for cyclohexene hydrogenation at low temperature using water as a solvent. The obtained results demonstrate remarkable efficiency of the synthesized material as a sustainable heterogeneous catalyst with very low amount of active species (Fe: 0.024 mol%), 90% conversion, high substrate/catalyst ratio (4157/1) as well as TON (3742) for 3 catalytic cycles. The present synthetic approach is highly green as it does not involve use of any noble metal, with no waste generation (E-factor = 0) as well as high reaction mass efficiency (92.20%).

As discussed in the general introduction, supported POMs have surpassing advantages of heterogeneous catalyst over the traditional disadvantages of POMs as homogeneous catalyst. Out of various supported POMs, phosphomolybdic acid (PMo_{12}) has gained more importance due to their excellent redox properties.

Phosphomolybdic acid (PMo_{12}) supported on various supports such as metal oxide active carbon [1, 2], metal organic framework [3-5], Al_2O_3 [6, 7], ionic liquid [8-10], polymer [11], various silica based materials [12-15] and zirconia (ZrO_2) [16-20] have gained increasing attention for oxidation of alkene and alcohols (styrene [7, 14, 15, 18-20], cis-cyclooctene [3, 11, 16] and benzyl alcohol [6, 14, 15, 20, 21]); hydrodesulphurization of thiophene [1, 10], dibenzothiophene [10], thioanisole [1, 10] and simulated oil [4]; esterification of acetic acid with hydroquinone [22], ethanol [12], n-butanol [17] and oleic acid with methanol [5]; dehydration of glycerol [23] and multicomponent synthesis of 2,4,5-trisubstituted imidazoles [24], tetrahydrobenzo[a]xanthene-11-ones [2] and b-acetamidoketones or esters [13].

As we mentioned in general introduction, PMo_{12} consist of two types of structure, primary anion and secondary structure. It was thought to take an advantage of modifying the secondary structure (available exchangeable protons) of PMo_{12} with transition metal which can lead to enhancement in catalytic activity. In this context, few reports are available on first row of transition metals (Co [25, 26], Fe [27] and Cu [28-30]) exchanged supported phosphomolybdic acid. However, above literature survey shows that only one report is available on Fe-doped $H_3PMo_{12}O_{40}$ immobilized on covalent organic frameworks (Fe/PMA@COFs) for cyclooctene epoxidation with reported by Lou group in 2019 [27].

Selective C=C hydrogenation is still challenging and fascinating to produce precursors for several intermediates using earth copious transition metals on industrial scale. Amongst, cyclohexene hydrogenation has gained significant importance as its hydrogenated product cyclohexane, is raw material for synthesis of cyclohexanol, cyclohexanone, which are further used in manufacturing of adipic acid and caprolactam, and moreover it is used as nonpolar solvent [31].

In the present chapter, we are reporting the designing of Fe exchanged phosphomolybdic acid supported on ZrO_2 and characterized thoroughly by various physicochemical techniques such as TGA, EDX, FT-IR, Raman spectroscopy, ESR, XPS, XRD and BET. Its catalytic efficiency was evaluated for cyclohexene hydrogenation at low temperature in water as a universal green solvent under mild conditions using molecular hydrogen as a reducing agent. For maximum conversion influence of different parameters were studied such as, catalyst amount, time, temperature, pressure and effect of solvents. Also, the heterogeneity test, as well as catalytic activity of the recycled catalyst, were performed under optimized conditions. The regenerated catalyst was characterized by EDX, FT-IR, ESR and XPS to confirm the stability of the catalyst. Green chemistry metrics were calculated and catalytic activity of the present catalyst was also compared with reported iron-based catalysts.

EXPERIMENTAL

Materials

All chemicals used were of A. R. grade. Phosphomolybdic acid ($H_3PMo_{12}O_{40}$), iron nitrate [$(Fe(NO_3)_3).9H_2O$], zirconium oxychloride ($ZrOCl_2 \cdot 8H_2O$), ammonia (25% w/v), cyclohexene and dichloromethane (DCM) were obtained from Merck and used as received.

Catalyst synthesis

Iron exchanged zirconia supported phosphomolybdic acid ($Fe\text{-}PMo_{12}/ZrO_2$) was synthesized by following three steps.

Step-1: Synthesis of Zirconia

Hydrous zirconia (ZrO_2) was synthesized following the same method reported by our group [7, 18]. Aqueous ammonia solution (12% w/v) was added to aqueous solution of $ZrOCl_2{\cdot}8H_2O$ (10% w/v) up to pH 8.5. The precipitates were aged at 100 °C on the water bath for 1 h, filtered, washed with conductivity water until a chloride free filtrate was obtained and dried at 100 °C for 10 h. The obtained material was designated as ZrO_2 (Scheme 1).

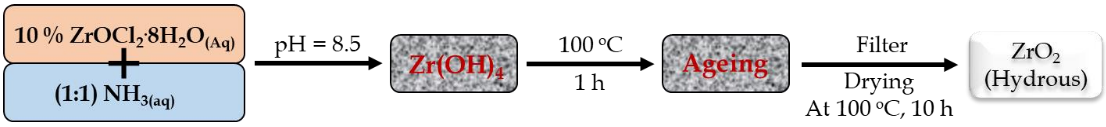

Scheme 1. Synthesis of hydrous zirconia

Step-2: Synthesis of phosphomolybdic acid supported on zirconia

30% phosphomolybdic acid supported on zirconia was synthesized by incipient wet impregnation method as reported earlier [18]. 1 g ZrO_2 was impregnated with an aqueous solution of PMo_{12} (0.3/30 g mL^{-1} of double distilled water) and dried for 10 hours at 100 °C after evaporation of the water from the suspension. The obtained light yellow colored material was designated as PMo_{12}/ZrO_2 (Scheme 2).

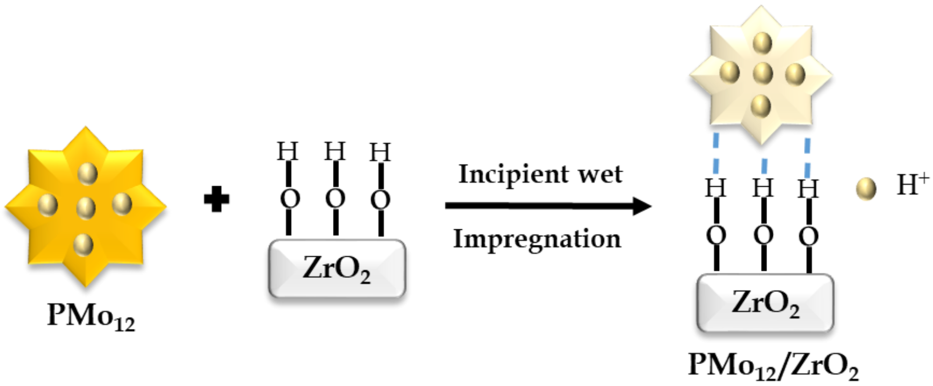

Scheme 2. Synthesis of Fe-PMo_{12}/ZrO_2

Step-3: Synthesis of Iron exchanged phosphomolybdic acid supported on zirconia

Iron exchanged phosphomolybdic acid supported on zirconia was synthesized by exchanging the available protons of PMo_{12} with iron. 1 g PMo_{12}/ZrO_2 was soaked in 25 mL 0.05 molar $Fe(NO_3)_3$ aqueous solution with interment stirring for 24 hours. The solution was filtered, washed with distilled water to remove excess iron and dried in air at room temperature. The obtained yellow colored material was designated as Fe-PMo_{12}/ZrO_2 (Scheme 3).

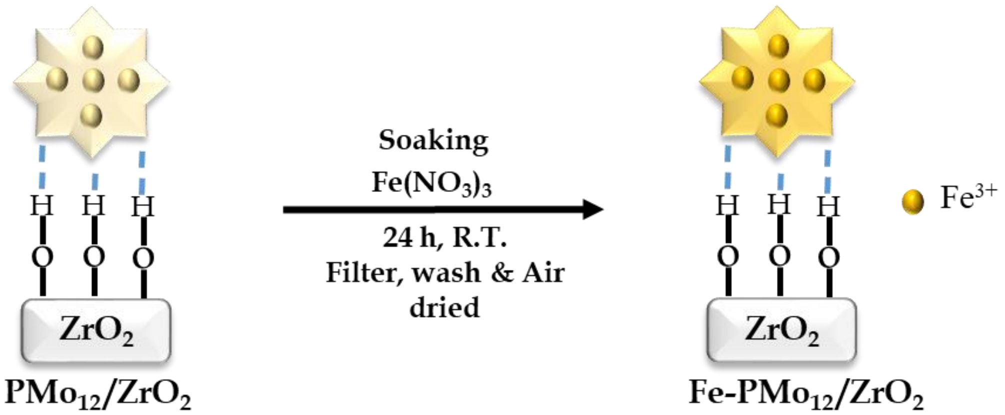

Scheme 3. Synthesis of Fe-PMo_{12}/ZrO_2

Catalytic activity

The catalytic reaction was performed in the high-pressure autoclave reactor. It was charged with 9.87 mmol of cyclohexene with 50 ml of water as a solvent and 25 mg of catalyst in the reactor vessel. The presence of air in the reactor vessel's unfilled piece is removed by several times flushed with H_2 gas. Finally, 10 bar H_2 pressure was applied for the reaction at 50 °C with a stirring rate of 500 rpm for three hours. The continuous reduction of pressure within the vessel was used to determine the progress of the reaction. After completion, the reaction mixture was cooled to room temperature and then H_2 pressure was released from the vent valve. The organic layer was extracted using dichloromethane, while the catalyst was collected from the liquid phase junction and finally recovered through centrifugation. The organic phase was dried with anhydrous magnesium sulfate and analyzed by a gas chromatograph (Shimadzu-2014) using a capillary column (RTX-5). The products were confirmed by comparison with the standard samples while conversion, selectivity and TON were calculated using equations given in general introduction. The catalytic methodology is schematically illustrated in Scheme 4.

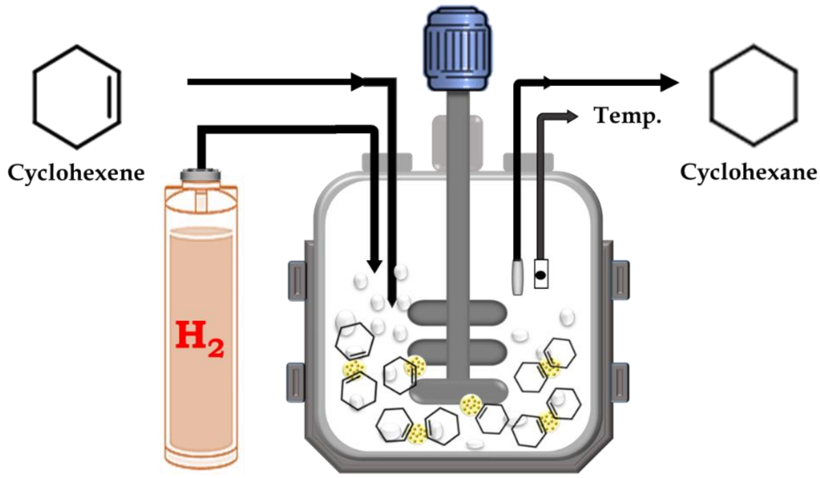

Scheme 4. Schematic illustration of cyclohexene hydrogenation reaction

RESULTS AND DISCUSSION

Please note that, we have not synthesized Fe nanoparticles in the case of Fe-PMo_{12}/ZrO_2 because as mentioned in chapter 1 formation Fe nanoparticles requires harsh condition such as high pressure, temperature and time. In these conditions, PMo_{12} gets reduced with decomposing of Keggin unit.

Characterization

The volumetric analysis of iron shows the presence of 0.53 wt% of Fe in Fe-PMo_{12}/ZrO_2. EDX mapping shows (Figure 1) presence of all the elements in the synthesized catalyst. EDX value of Fe (0.54 wt%) and Mo (14.05 wt%) are in good agreement with the theoretically calculated value of Fe (0.57 wt%) and Mo (14.14 wt%). Further, ICP-OES analysis also confirmed that the Fe (0.59%) and Mo (14.19%) contents were present in synthesized material, which is good agreement with calculated one. Here, the low amount of Fe, indicates that Fe is exchanged only with the available protons of PMo_{12}/ZrO_2.

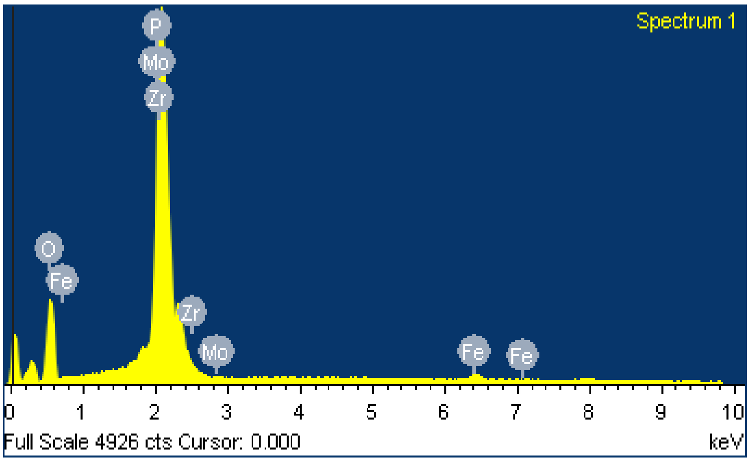

Figure 1. EDX mapping of Fe-PMo_{12}/ZrO_2

TGA curve of PMo_{12}/ZrO_2 shows (Figure 2) 5.3% weight loss up to 100 °C, which is attributed to the loss of adsorbed water. Further, it shows 6.4% weight loss up to 300 °C corresponding to the loss of crystalline water molecules present in PMo_{12}. After that, no further weight loss up to 500 °C indicates the stability of PMo_{12}/ZrO_2. TGA of Fe-PMo_{12}/ZrO_2 shows 9.3% weight loss up to 100 °C due to the adsorbed water. No weight loss observed up to 500 °C indicating the stability up to 500 °C.

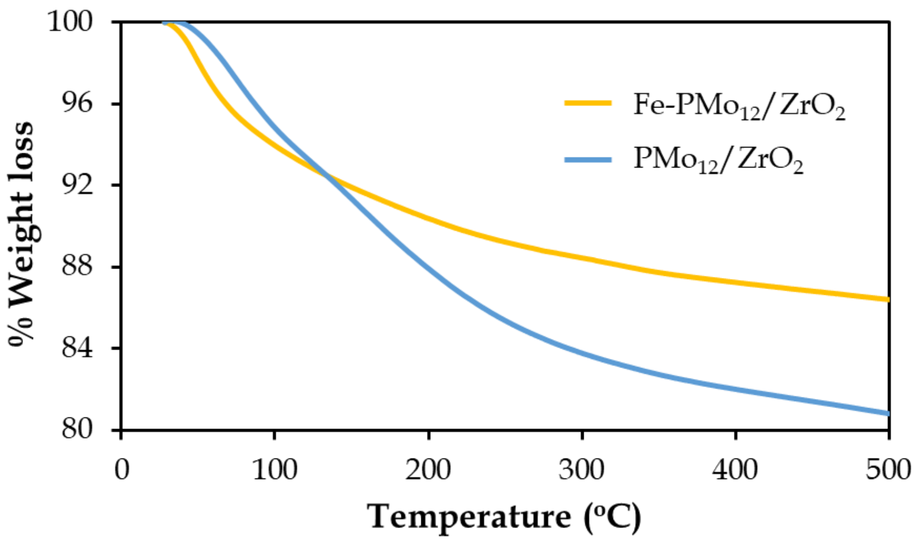

Figure 2. TGA curves of PMo_{12}/ZrO_2 and Fe-PMo_{12}/ZrO_2

The FT-IR spectra of ZrO_2, PMo_{12}, PMo_{12}/ZrO_2 and Fe-$PMo_{12}/$ ZrO_2 are displayed in figure 3. In the spectra of ZrO_2 (Figure 3a), characteristic broad band at 1631 and 1370 cm^{-1} were observed for H-O-H asymmetric stretching, and O-

H-O bending vibrations respectively, and broadband at 700-400cm^{-1} was observed corresponding to Zr-O-H bending vibrations [19, 20, 31]. The FT-IR spectrum of PMo_{12} shows all the (Figure 3b) characteristic bands at 1060 cm^{-1} (P-O_a), 965 cm^{-1}(M=O), 870 cm^{-1} (Mo-O_b-Mo) and 790 cm^{-1} (Mo-O_c-Mo) [7, 18]. In figure 3c, PMo_{12}/ZrO_2 shows all characteristic bands of PMo_{12} at 1075 cm^{-1} (P-O_a), 948 cm^{-1}(M=O_t) and 887 cm^{-1} (Mo-O_b-Mo) as well as ZrO_2 at 1620 cm^{-1} H-O-H, 1381 cm^{-1} O-H-O and broadband at 700-600 cm^{-1} (Zr-O-H) [18]. Similarly, Fe-PMo_{12}/ZrO_2 shows all the characteristic bands of PMo_{12}/ZrO_2 with minor shifts, attributed to the change in the counter cation environment of PMo_{12}. An additional band of Fe-O stretching has appeared at 509 cm^{-1} which confirms that only iron is exchanged with the proton of PMo_{12}.

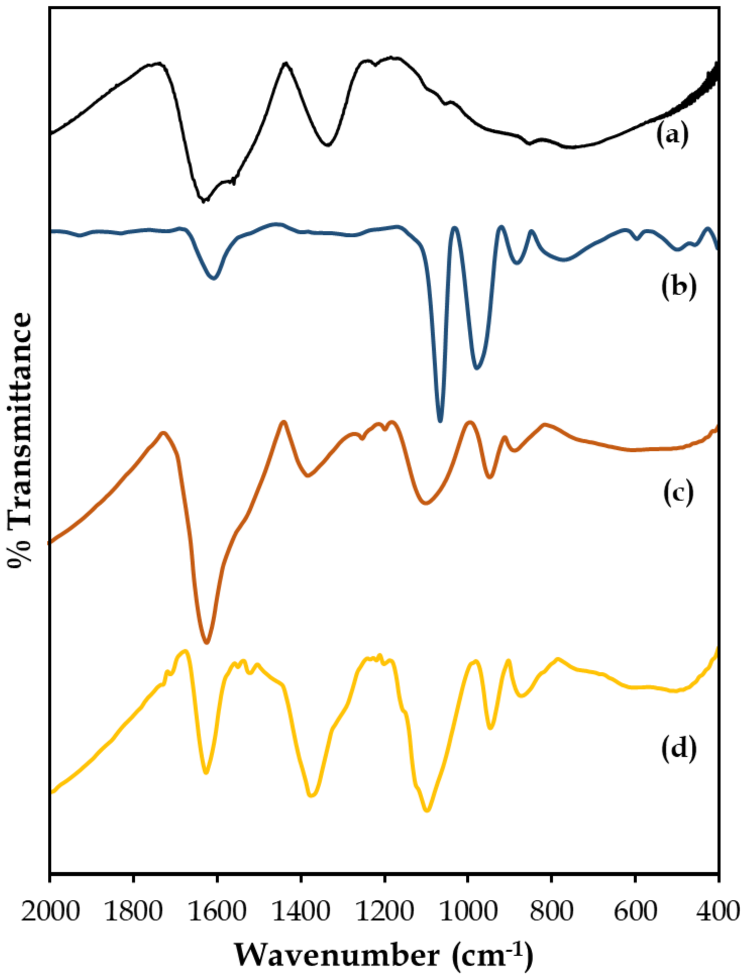

Figure 3. FT-IR spectra of (a) ZrO_2, (b) PMo_{12}, (c) PMo_{12}/ZrO_2 and (d) Fe-PMo_{12}/ZrO_2

Table 1. Raman Data of ZrO_2, PMo_{12}, PMo_{12}/ZrO_2 and Fe-PMo_{12}/ZrO_2

Catalyst	$Mo=O_t$	$Mo-O_b-Mo$	$Mo-O_c-Mo$	$Mo-O_a$	O-Zr–O
ZrO_2	-	-	-	-	187, 345
PMo_{12}	v_s1005, v_{as} 987	v_{as} 916	v_{as} 620	v_{as} 251	-
PMo_{12}/ZrO_2	v_s 969, v_{as} 944	v_{as} 920	v_{as} 625	v_{as} 212	-
Fe-PMo_{12}/ZrO_2	v_s 947, v_{as} 937	v_{as} 896	v_{as} 603	v_{as} 225	-

The Raman data of ZrO_2, PMo_{12}, PMo_{12}/ZrO_2 and Fe- PMo_{12}/ZrO_2 are shown in table 1 and figure 4. ZrO_2 (Figure 4a) shows two broad bands at 187 and 345 cm^{-1} which are associated with its hydrated amorphous state [32, 33]. The Raman spectra of PMo_{12} (Figure 4b) show bands at 1005 and 987 cm^{-1} corresponding to symmetric and asymmetric vibration of $Mo=O_t$ respectively. Other observed bands at 916, 620 and 251 cm^{-1} corresponds to asymmetric vibrations of corner-sharing $Mo-O_b-Mo$, edge-sharing $Mo-O_c-Mo$ and $Mo-O_a-P$ stretching respectively [34]. PMo_{12}/ZrO_2 (Figure 4c) show all characteristic bands of PMo_{12} with shifting at 969, 944, 920, 625 and 212 cm^{-1} corresponding to v_s $Mo=O_t$, v_{as} $Mo=O_t$, v_{as} $Mo-O_b-Mo$, $v_{as}Mo-O_c-Mo$ and $v_{as}Mo-O_a-P$ respectively [34]. The significant shift may be due to the interaction between PMo_{12} and ZrO_2. Similarly, from the Raman data, after exchanging the counter proton with Fe (Fe-PMo_{12}/ZrO_2) shows the presence of all characteristic bands of PMo_{12}/ZrO_2 with the shift at 949, 937, 896, 603 and 235 cm^{-1} corresponding to v_s $Mo=O_t$, v_{as} $Mo=O_t$, v_{as} $Mo-O_b-Mo$, $v_{as}Mo-O_c-Mo$ and $v_{as}Mo-O_a-P$ respectively. The observed shifting may be due to the exchange of available protons of PMo_{12}/ZrO_2 by Fe.

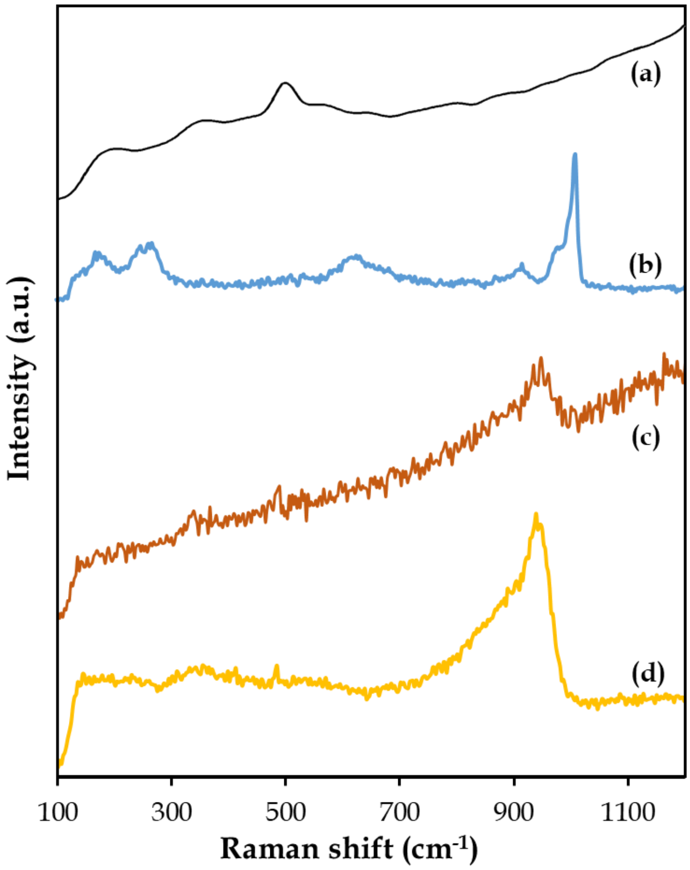

Figure 4. Raman spectra of (a) ZrO_2, (b) PMo_{12}, (c) PMo_{12}/ZrO_2 and (d) Fe-PMo_{12}/ZrO_2

^{31}P MAS NMR of PMo_{12}, PMo_{12}/ZrO_2 and Fe-PMo_{12}/ZrO_2 was carried to understand the chemical environment surrounding the central phosphorus of PMo_{12}. ^{31}P MAS NMR of PMo_{12} (Figure 5a) shows a peak at -3.8 ppm which is in good agreement with the reported one [35, 36]. While in case of PMo_{12}/ZrO_2, the peak was obtained at -4.1 ppm (Figure 5b), the observed shift may be due to the strong interaction between PMo_{12} and ZrO_2. Whereas in Fe-PMo_{12}/ZrO_2, the peak was obtained at -5.13 (Figure 5b), the observed significant upfield shift may be due to the exchange of Fe with available counter protons and similar effect was also observed for Pt-Exchanged PMo_{12} supported on activated carbon [37, 38]. Also, it is important to note that Fe gets exchanged with the outer proton only and does not go into the lacuna. If it would have been inside the lacuna, it should not show any NMR peak [36].

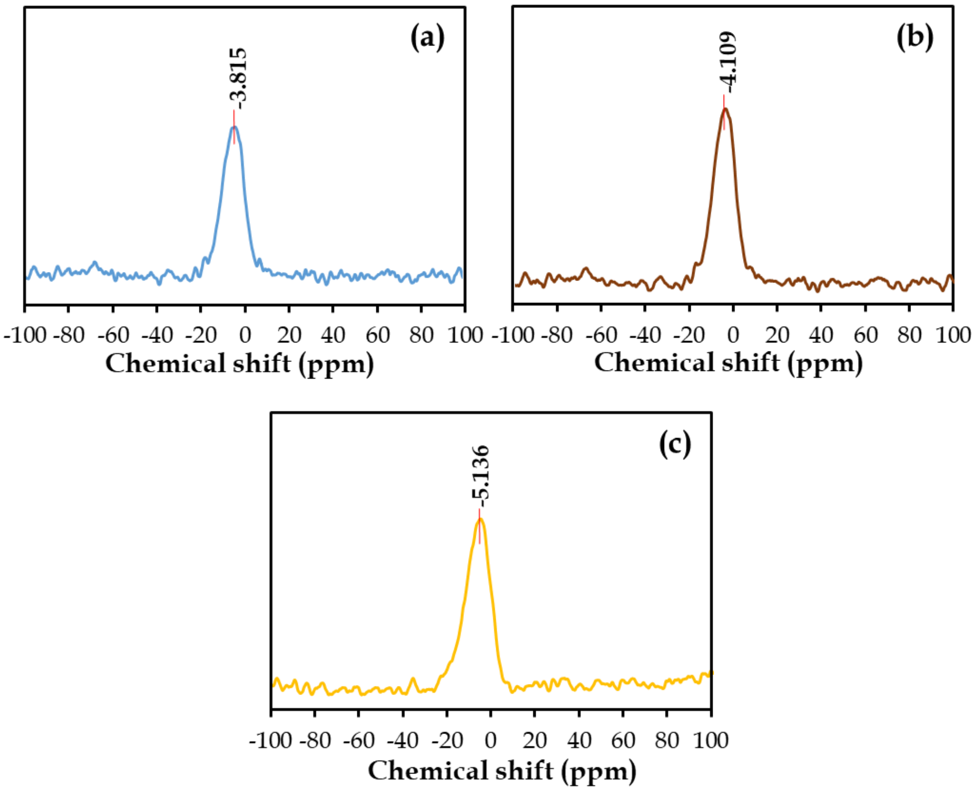

Figure 5. ^{31}P MAS NMR of (a) PMo_{12}, (b) PMo_{12}/ZrO_2 and (c) Fe-PMo_{12}/ZrO_2

Figure 6a shows the full range (5000–2500 G) X-band liquid nitrogen temperature ESR spectrum for Fe-PMo_{12}/ZrO_2. It gave a single isotropic hyperfine spectrum at g= 4.3 for Fe in +3 states with distorted octahedral geometry and it incorporated with phosphomolybdate in high-spine (3+ state) [36]. The presence of Fe^{3+}, which is further confirmed by XPS.

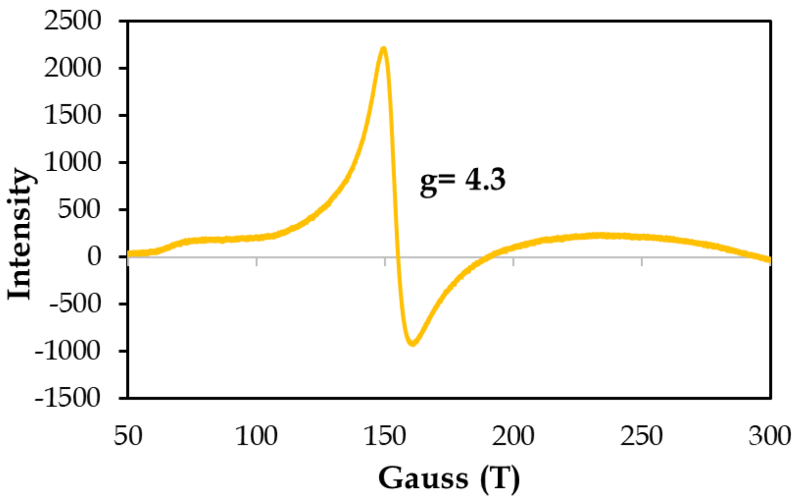

Figure 6. ESR spectrum of Fe-PMo_{12}/ZrO_2

XPS of Fe-PMo_{12}/ZrO_2 shows (Figure 7) the binding energy peak at 724 eV corresponding to $Fe2p_{1/2}$ energy level, confirming the presence of Fe^{3+} [27, 39]. Similarly, the binding energy level for Mo^{6+} was observed as two doublet i) at 233 and 235 eV corresponding to $3d_{5/2}$ and $3d_{3/2}$ energy levels ii) at 397 and 416 eV respectively for $3p_{3/2}$ and $3p_{1/2}$ energy level [34]. Two additional intense peaks at binding energy 331 eV and 345 eV are attributed to $Zr3p_{3/2}$ and $Zr3p_{1/2}$ [31, 33]. Also, a highly intense binding energy peak at 532 eV attributed to O1s for oxygen present in PMo_{12} as well as ZrO_2. This XPS confirms the presence of Mo^{6+}, Fe^{3+} and Zr^{4+} in the synthesized catalyst.

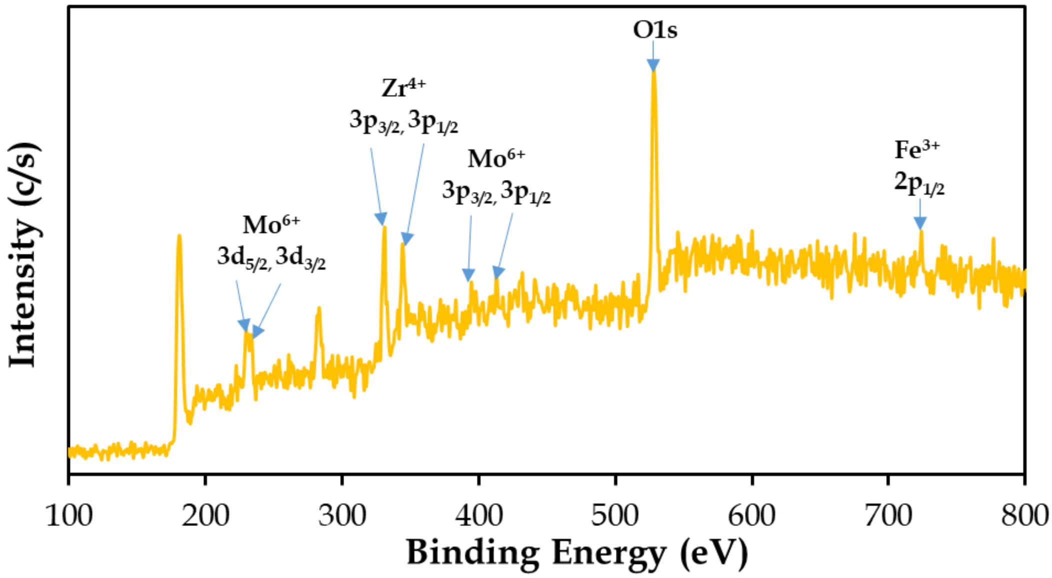

Figure 7. XPS of Fe-PMo_{12}/ZrO_2

The BET surface areas of ZrO_2, PMo_{12}/ZrO_2 and Fe- PMo_{12}/ZrO_2 were shown in figure 8. The BET surface area of ZrO_2 is 146 m^2 g^{-1} [32, 33] whereas the surface area of PMo_{12}/ZrO_2 is 204 m^2 g^{-1}, which is significantly higher as compared to support ZrO_2 because of the strong interaction between PMo_{12} and support [7]. However, the surface area of Fe-PMo_{12}/ZrO_2 was found to be 208 m^2 g^{-1}, this may be due to the exchange of Fe with available protons of PMo_{12}. The nitrogen adsorption-desorption isotherms of PMo_{12}/ZrO_2 and Fe- PMo_{12}/ZrO_2 are almost similar (Figure 8), confirms that there is no change in the basic structure.

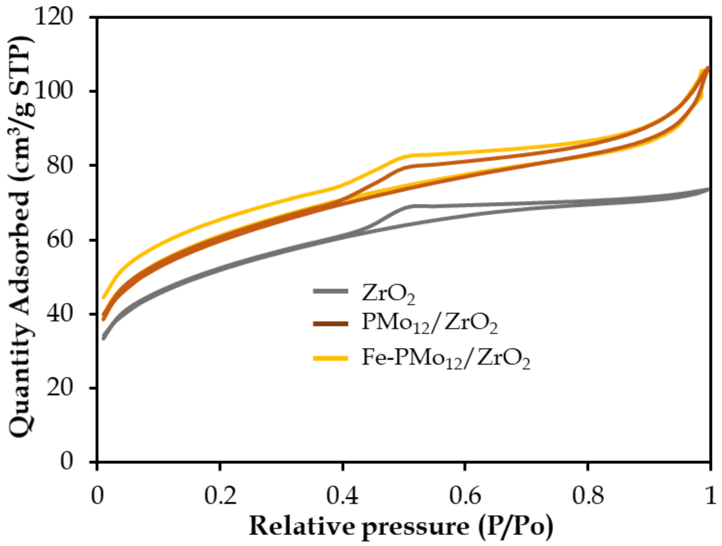

Figure 8. N_2 adsorption desorption isotherm of ZrO_2, PMo_{12}/ZrO_2 and Fe-PMo_{12}/ZrO_2

The powder XRD of ZrO_2, PMo_{12}, PMo_{12}/ZrO_2 and Fe-PMo_{12}/ZrO_2 are shown in figure 9. The powder XRD of ZrO_2 shows amorphous nature of support. PMo_{12} shows all characteristic peaks in the range of 15^0 to 35^0 of 2θ [7] . The XRD pattern of PMo_{12}/ZrO_2 does not show the characteristics peak of PMo_{12}, which suggested that the PMo_{12} is highly dispersed in a non-crystalline form on the support (ZrO_2) [34]. The XRD pattern of Fe-PMo_{12}/ZrO_2 is quite similar to PMo_{12}/ZrO_2, indicating that Fe highly is depressed on non-crystalline PMo_{12}/ZrO_2.

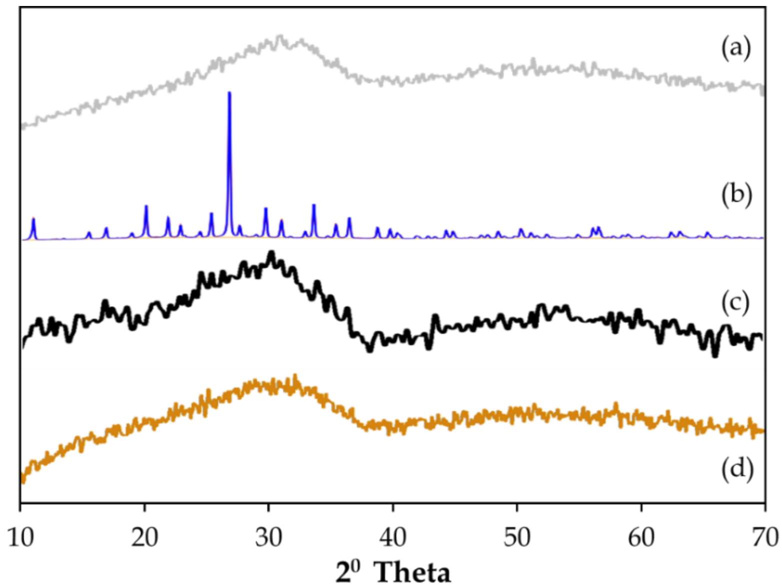

Figure 9. Powder XRD of (a) ZrO_2, (b) PMo_{12}, (c) PMo_{12}/ZrO_2 and (d) Fe-PMo_{12}/ZrO_2

HAADF-STEM images of Fe-PMo_{12}/ZrO_2 (Figure 10) also confirm the homogeneous dispersion of Fe over the PMo_{12}/ZrO_2.

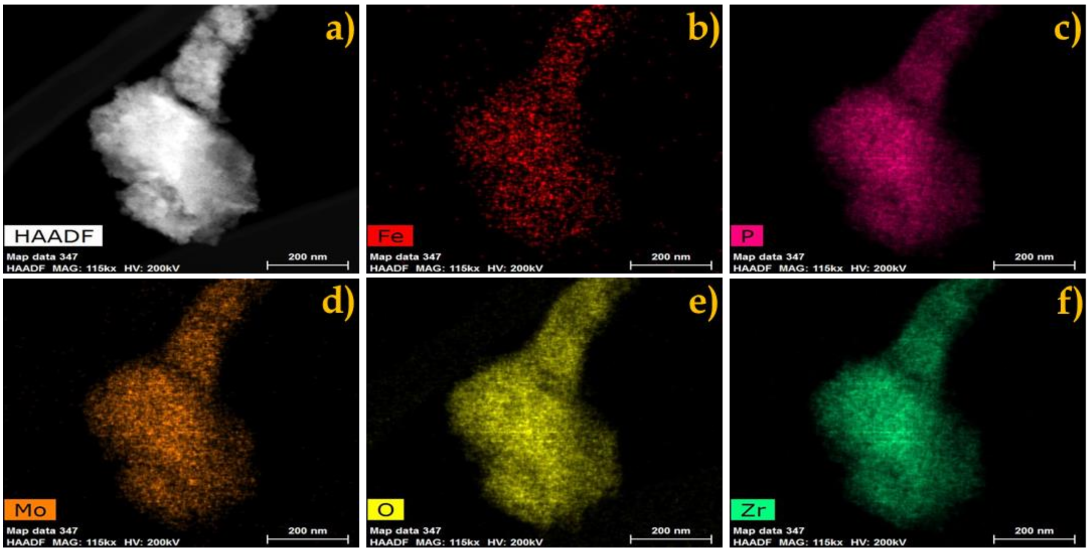

Figure 10. (a)HAADF STEM and (b-f) EDX images of Fe-PMo_{12}/ZrO_2

In summary, from FT-IR, Raman and ^{31}P NMR spectra it is seen that PMo_{12} structure is retained even after supporting on support and exchange of Fe. From ESR and XPS confirmed that the Fe and Mo present in a +3 state and 6+ respectively. BET, XRD and HAADF-STEM showed that iron highly dispersed on the surface of PMo_{12}/ZrO_2.

Catalytic activity

The catalytic activity of the synthesized catalyst was evaluated towards the hydrogenation of cyclohexene (Scheme 4). To optimize the conditions for maximum conversion, the effect of different reaction parameters such as catalyst amount, temperature, pressure, time and solvent were studied.

The obtained results for the effect of solvent on conversion show (Table 2) low conversion (29%) with acetonitrile which may be due to its oxidizing nature, and resistance to cyclohexene reduction. The catalyst was found to be moderately active in the presence of protic solvent such as ethanol and methanol due to its reducing nature. However, the catalyst was surprising found to be highly active in the case of water as solvent (i.e., 90%), due to its hydrophobic nature and on water effects. Therefore, water was chosen as a solvent to carry out further studies.

Table 2. Effect of solvent

Solvent(ml)	%Conversion	%Selectivity
Acetonitrile	29	100
EtOH	56	100
MeOH	76	100
Water	90	100

Reaction conditions: Catalyst (25 mg), cyclohexene (9.87 mmol), solvent (50 mL), H_2 pressure (10 bar), temperature (50 °C).

The effect of catalyst amount was investigated by varying the amounts from 5 to 30 mg, as shown in figure 11a. Initially, an increase in catalyst amount up to 25 mg also increases % conversion. The obtained result can be attributed to an increase in active sites i.e., Fe within catalyst amount. Moreover, further increase in catalyst amount (>25 mg) did not show a significant change in conversion due to blocking of the active sites. Therefore, 25 mg catalyst amount is optimized for maximum conversion (90%).

The effect of hydrogen pressure was also screened between 5 and 10 bar (Figure 11b). The obtained result shows that the %conversion of cyclohexane also increased linearly with increase in H_2 pressure from 5 bar to 10 bar. This suggests that the rate of reaction is also dependent on H_2 pressure. H_2 pressure of 10 bar is optimized for the optimum rate of reaction.

Effect of time on reaction conversion was screened between 1 to 6 h (Figure 11c). The obtained result shows that with an increase in time, % conversion also increases up to 2h which is in good agreement with the well-known fact that the formation of reactive intermediates from reactants increases with an increase in time and convert to product. With further prolonging the reaction up to 6h, no significant change in conversion was observed. Therefore, 2 h reaction time was optimized for 90 % conversion.

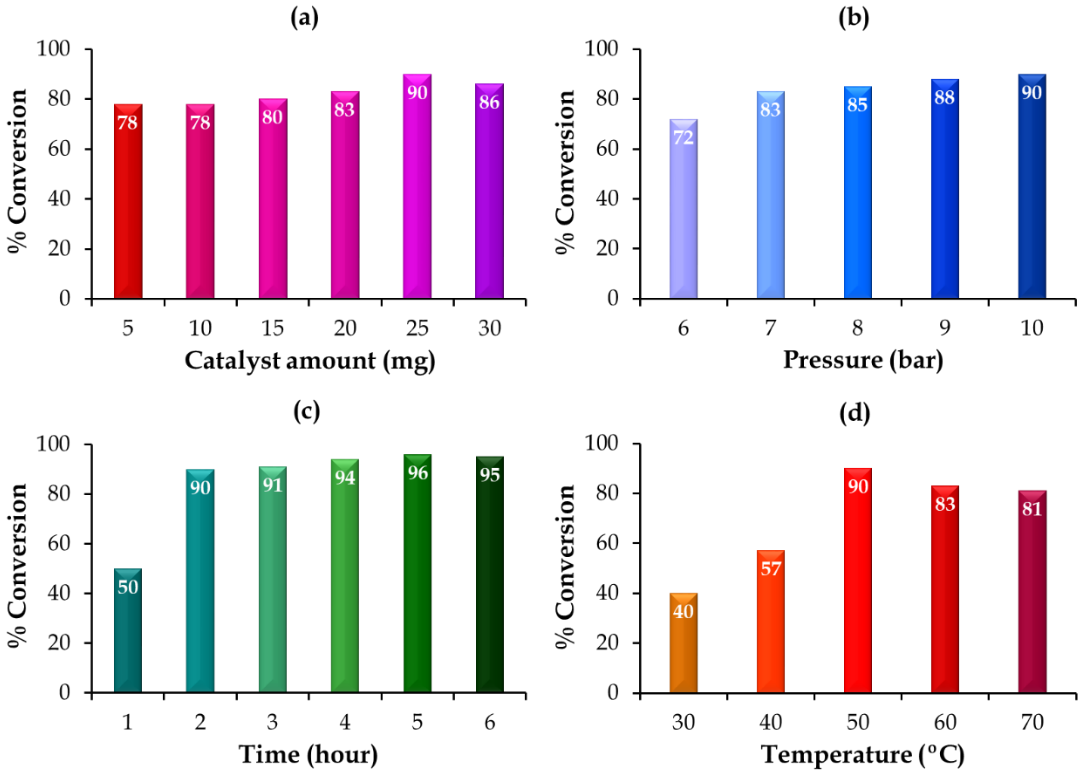

Figure 11. Optimization of reaction parameters for cyclohexene hydrogenation. Reaction conditions: (a) Effect of catalyst amount- Cyclohexene (9.87 mmol), H_2O (50 mL), H_2 pressure (10 bar), Time (2 h), temperature (50 °C); (b) Effect of H_2 pressure- Catalyst (25 mg), cyclohexene (9.87 mmol), H_2O (50 mL), time (2 h), temperature (80 °C); (c) Effect of time- Catalyst (25 mg), cyclohexene (9.87 mmol), H_2O (50 mL), H_2 pressure (10 bar), temperature (50 °C); (d) Effect of temperature: Catalyst (25 mg), cyclohexene (9.87 mmol), H_2O (50 mL), H_2 pressure (10 bar), time (2 h).

The influence of reaction temperature was studied in the range of 30 °C to 70 °C with an interval of 10 °C. Obtained result (Figure 11d) shows that % conversion increased from 30 °C to 50 °C. However, further increase in temperature shows a gradual decrease in % conversion, this may be due to the progress of the reversible process. Maximum 90% conversion was achieved at 50 °C.

The optimized conditions for the maximum % conversion (90) with 3742 TON is: catalyst amount (25 mg; Fe: 0.024 mol%), cyclohexene (9.87 mmol), H_2O (50 mL), H_2 pressure (10 bar), time (2 h) and temperature (50 °C), and Substrate/Catalyst ratio (4157/1).

The gas chromatograph of optimized reaction condition for cyclohexene hydrogenation are shown in figure 12.

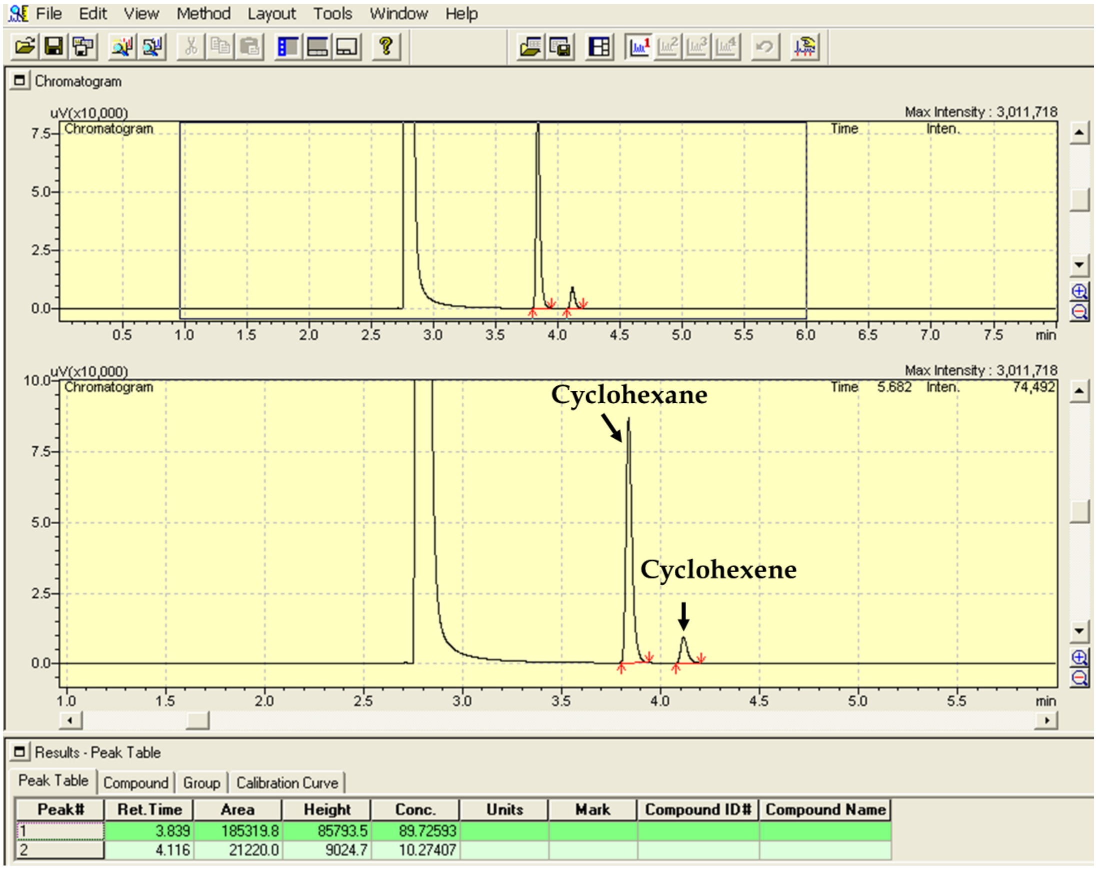

Figure 12. Gas chromatograph of cyclohexene hydrogenation

Control experiment

The result of the control experiment with ZrO_2, PMo_{12}/ZrO_2, $Fe(NO_3)_3$, Fe/ZrO_2 and $Fe\text{-}PMo_{12}/ZrO_2$ was performed under optimized conditions and the obtained results are shown in table 3. There was no product formation with ZrO_2 and PMo_{12}/ZrO_2 because they are inactive, which indicates that Fe is only the responsible real active species for the said reaction conversion. It is interesting to note that there was quite a large difference in % conversion for $Fe(NO_3)_3$ (Homogeneous), Fe/ZrO_2 (Heterogeneous) and $Fe\text{-}PMo_{12}/ZrO_2$ (Heterogeneous) were observed. This may be due to the fact that during the reaction, $Fe(NO_3)_3$ sticks to the sidewalls of the reaction vessel (Figure 13) and therefore the conversion was lower. While, in Fe/ZrO_2 and $Fe\text{-}PMo_{12}/ZrO_2$ the catalyst moves freely during the reaction and does not stick to the vessel, giving 78% and 90% conversion respectively.

Table 3. Control experiment

Catalyst	%Conversion	%Selectivity
[a]ZrO_2	-	-
[b]PMo_{12}/ZrO_2	-	-
[c]$Fe(NO_3)_3$	39	100
[d]Fe/ZrO_2	78	100
[d]$Fe\text{-}PMo_{12}/ZrO_2$	90	100

Reaction conditions: catalyst ([a]19 mg, [b]24.8 mg, [c]1.32 mg and [d]25 mg; Fe: 0.024 mol%), cyclohexene (9.87 mmol), H_2O (50 mL), H_2 pressure (10 bar), time (2 h) and temperature (50 °C).

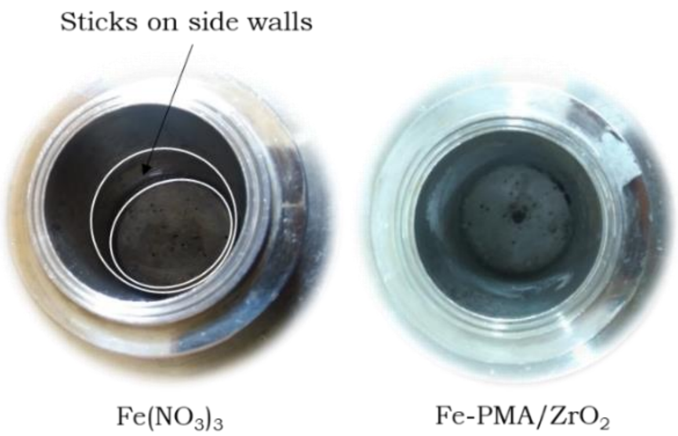

Figure 13. Reaction vessel image after completion of the reaction

Hot filtration and heterogeneity test

The strength of the catalyst during the reaction is highly essential, as it would decrease the attractiveness of the catalyst if the active species are leached out. To check heterogeneity of $Fe\text{-}PMo_{12}/ZrO_2$ and Fe/ZrO_2, hot filtration test was carried out, in which the reaction was performed under optimized conditions for one hour, then the catalyst was removed, and the reaction was continued for 2h using the filtrate. The resulting reaction mixture was extracted with dichloromethane and analyzed by gas chromatography. The obtained result for Fe-PMo_{12}/ZrO_2 shows (Table 4) no significant change in the % conversion, which indicates that there was no leaching of iron during the reaction and the catalyst is truly heterogeneous. Whereas in case of Fe/ZrO_2 significant change in the % conversion was observed, which indicates the presence of active spices in the reaction, showing that there was leaching of iron during the reaction and the catalyst is not truly heterogeneous. Further, it confirms that PMo_{12} stabilize Fe. To confirm that there is no leaching of iron and heterogeneity of Fe-PMo_{12}/ZrO_2, the regenerated catalyst was characterized by EDX (Figure 10) and reaction mixture by atomic absorption spectroscopy (AAS). No loss in Fe content (0.55 wt%) confirms the true heterogeneous nature of the catalyst, which is also reflected in the recycling study.

Table 4. Hot filtration test

Catalyst	% Conversion
[a]Fe-PMo_{12}/ZrO_2	52 (after one hour)
	53 (after two hour)
[b]Fe/ZrO_2	46 (after one hour)
	51 (after two hour)

Reaction conditions: Catalyst (25 mg; [a,b]Fe: 0.024 mol%), cyclohexene (9.87 mmol), H_2O (50 mL), H_2 pressure (10 bar), time (2 h) and temperature (50 °C).

Regeneration and recycling studies

The recovery and recyclability of the catalyst is a key issue for the sustainability of any catalytic process. After completion of the reaction, the organic layer was extracted by dichloromethane and the catalyst was regenerated through simply centrifuging, washed with dichloromethane followed by water and then air-dry and finally used for the next cycle. The regenerated catalyst is used for the next cycle under optimized conditions and obtained results (Table 5) did not show any change in % conversion up to three cycles, which indicating that catalyst was stable, truly heterogeneous, can be regenerated and reused for further catalytic runs also.

Table 5. Recycling studies

Catalyst	% Conversion	TON number
Fresh catalyst	90	3742
Recycled-1	89	3742
Recycled-2	89	3742
Recycled-3	88	3741

Reaction conditions: Catalyst (25 mg), cyclohexene (9.87 mmol), H_2O (50 mL), H_2 pressure (10 bar), time (2 h) and temperature (50 °C)

Characterization of regenerated catalyst

To check retention of the regenerated catalyst Fe-PMo_{12}/ZrO_2 structure EDX, ICP, FT-IR, ESR and XPS analyses were performed.

EDX mapping (Figure 14) confirmed the presence of all elements. EDX value of Fe(0.55 wt%) and Mo (14.15 wt%) as well as ICP value of Fe (0.59%) and Mo (14.19%) of regenerated Fe-PMo_{12}/ZrO_2 are in good agreement with the fresh one, indicating that there was no leaching of Fe during the reaction and regeneration of the catalyst.

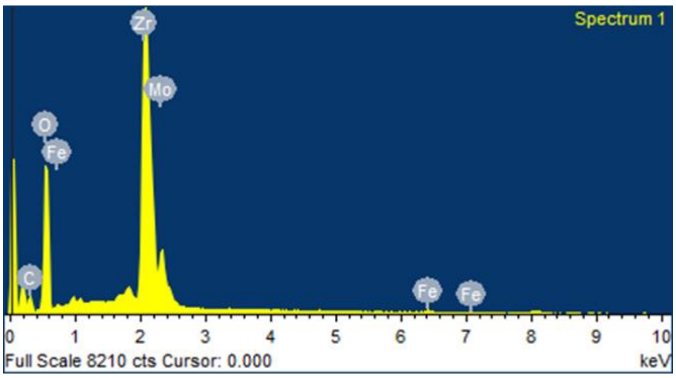

Figure 14. EDX mapping of regenerated Fe-PMo_{12}/ZrO_2

The FT-IR spectrum of fresh Fe-PMo_{12}/ZrO_2 and regenerated Fe-PMo_{12}/ZrO_2 are (Figure 15) almost identical, without any significant shift in the bands. This indicates that the structure of the catalyst remains unchanged even after regeneration. However, in terms of intensity, the spectrum is slightly different from the fresh one. This could be due to the sticking of the substrates on the surface of the catalyst, although it does not affect the reusability of the catalyst.

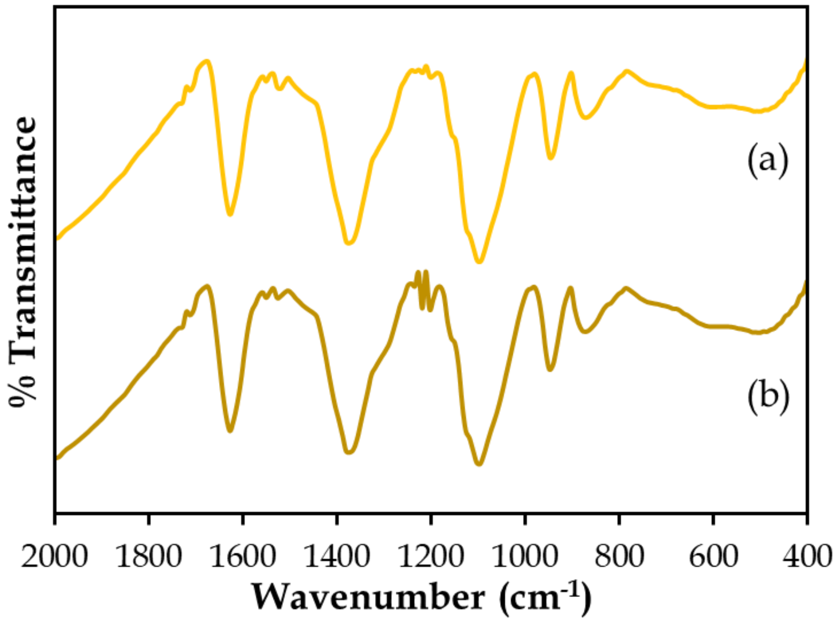

Figure 15. FI-IR spectra of (a) fresh Fe-PMo_{12}/ZrO_2 and (b) regenerated -Fe-PMo_{12}/ZrO_2

ESR spectra of regenerated Fe-PMo_{12}/ZrO_2 gives a single hyperfine spectrum (Figure 16) with an isotropic signal at g=4.3, which is identical with fresh catalyst. Obtained result confirmed that Fe is present in a +3 state and remains intact even after regeneration.

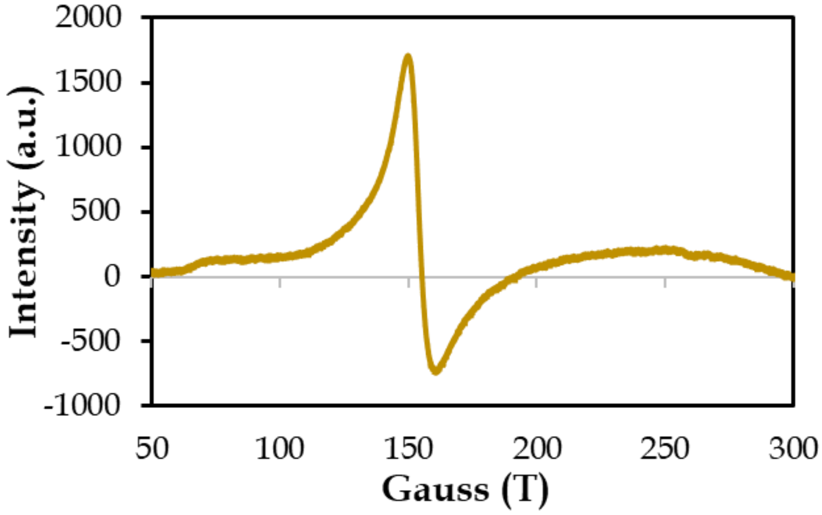

Figure 16. ESR spectra of regenerated Fe-PMo_{12}/ZrO_2

XPS spectrum of regenerated Fe-PMo_{12}/ZrO_2 (Figure 17) shows all identical peaks as that of fresh Fe-PMo_{12}/ZrO_2. This further confirmed that during hydrogenation reaction as well as regeneration of catalyst Fe and Mo does not get reduced or leached out of the catalyst.

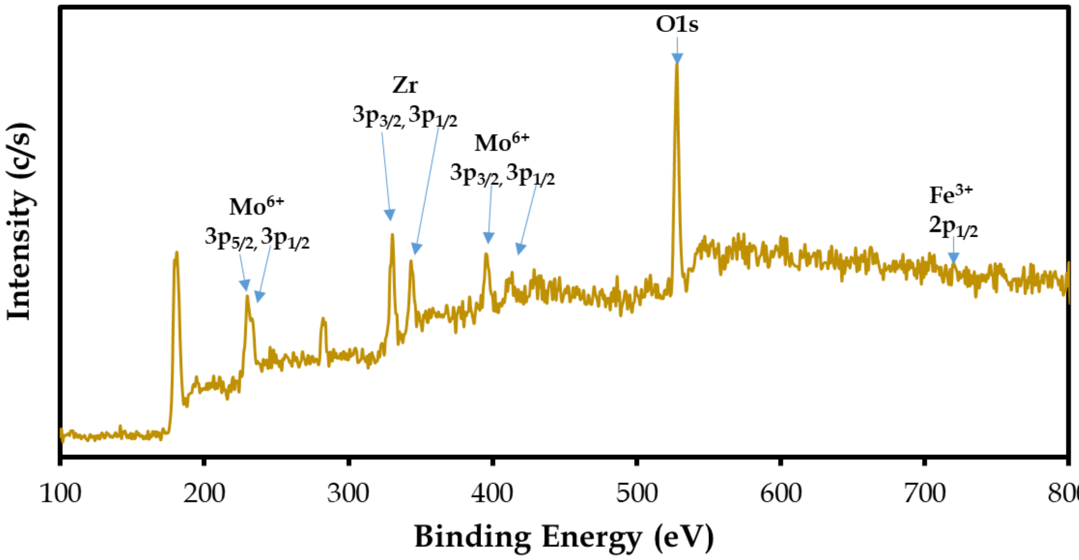

Figure 17. XPS spectra of regenerated Fe-PMo_{12}/ZrO_2

Mechanistic investigation

Based on the results (Table 6), we are proposing the same well-known hydride transferred mechanism in the present work (Scheme 5). As seen in the control experiment (Table 4), Fe is the only active species where molecular hydrogen initially gets adsorbed onto the Fe surface to form Fe-H. This formed species subsequently transfers the hydrogen to the unsaturated bond of adsorbed cyclohexene over the surface of Fe to form the product cyclohexane.

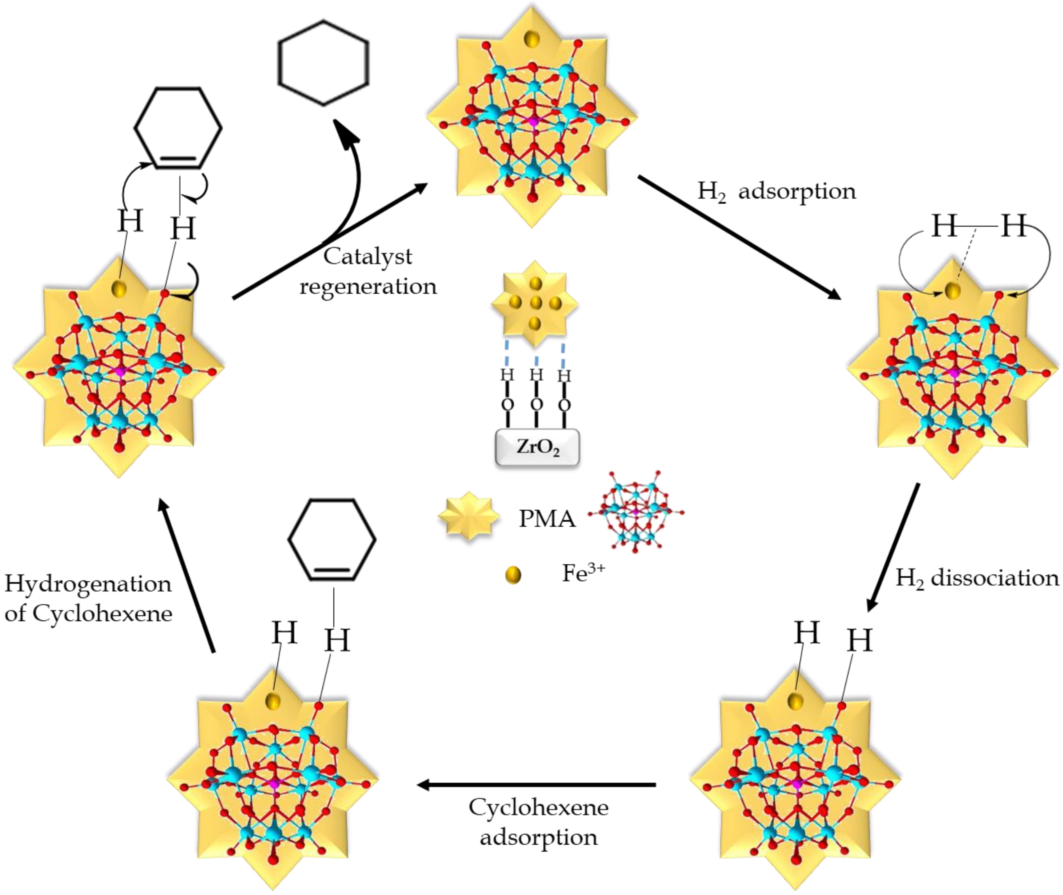

Scheme 5. Probable reaction mechanism for cyclohexene hydrogenation

Viability of the catalyst

To see the viability of the existing catalyst, hydrogenation of various substrates over Fe-PMo_{12}/ZrO_2 was carried out under optimized conditions and the obtained results are shown in table 6. The catalyst shows appreciable reactivity towards aromatic, cyclic alkenes as well as nitro group (-NO_2) with a good conversion rate. However, the observed low % conversion for the non-planar cyclic alkene may be due to the difficulties to approach the catalytic site due to steric hindrance during the reaction. Moreover, the catalyst was found to be active for selective hydrogenation of the C=C bond without affecting the C=O bond when simultaneously present in the substrates. In other variation hydrogenation of levulinic acid gave 0% of conversion. As mentioned in chapter 1, it requires harsh reaction conditions.

Table 6. Substrate study

Substrate	Product	% Conversion
	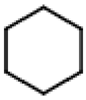	90
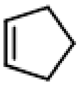	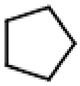	86
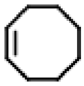	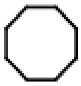	66
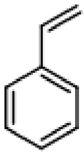	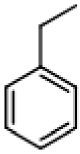	98
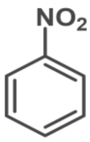	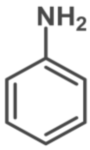	81
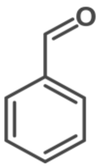	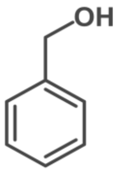	49
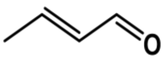	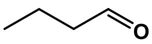	76
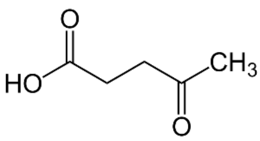	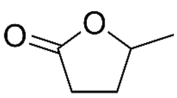	0

Reaction conditions: Catalyst (25 mg; 0.024 mol%), substrate (9.87 mmol), H_2O (50 mL), H_2 pressure (10 bar), time (2 h) and temperature (50 °C).

Comparison with reported catalysts

The catalytic activity of the present catalyst is compared with reported catalysts (Table 7). There are no reports for complete optimization of cyclohexene hydrogenation by Fe catalyst, comparison was carried out with reported Fe based catalyst where hydrogenation of cyclohexene was mentioned only in substrate study. Johannes et al. (Entry 1 & 2) reported in THF solvent with 5 mol% of catalyst at 1bar and 20 bar giving the same conversion (22% at r.t. and 100% at 100 ^{o}C). While Breit et al. (Entry 3) has reported 74% conversion with 0.9 mol% of Fe catalyst in almost similar reaction condition reported by Johannes et al. whereas, Chaudret et al. achieved high conversion (99%) using mesitylene as a solvent with very high pressure of H_2 (20 bar) and time (20 h) compared to the present catalytic system. As seen in table 6, the advantage of the present catalyst lies in giving excellent conversion (90%) with lower 0.024 mol% of Fe as well as lower reaction time and temperature. Also, it is important to note that the catalyst shows remarkable reactivity in terms of TON number in water as a green solvent compared to all the other reported catalysts.

Table 7. Comparison with reported catalyst

Entry	Catalyst	Fe (mol%)	Solvent	H_2 pressure (bar)	Temp. (°C)	Time (h)	% Conversion	TON
1	Fe-NPs [40]	5	THF	1	(r.t./ 100)	15	22/100	20
2	$FeCl_3$/EtMgCl [41]	5	THF	20	(r.t./ 100)	18	22/100	20
3	FeNP/CDG [42]	0.9	THF	20	100	24	74	111
4	Iron(0)-NPs [43]	0.25	Mesitylene	20	r.t.	20	>99	42
5	**Present work**	**0.024**	**Water**	**10**	**50**	**2**	**90**	**3742**

CONCLUSION

- **Fe-PMo_{12}/ZrO_2** was designed via two steps wet-impregnation as well as **ion-exchanged** method and **characterized** by various physicochemical techniques.
- The obtained results depict that very **small amount of active species** (0.024 mol% Fe) is **sufficient** for hydrogenation to achieve **high conversion** (90 %) and **TON** (3742) using **water** as a **green solvent**.
- The catalyst was **recycled** and **reused** up to **three catalytic cycles** without significant change in **activity, leaching or degradation.** It was further confirmed by the **characterization of recycled catalyst.**
- The designed catalyst is extremely **viable** towards **various substrates**. **Comparison** with reported catalysts shows that the present one is **superior** in terms of **conversion, active amount of Fe, reaction conditions and TON.**

Comparison study of $PMo_{11}Fe$ and Fe-PMo_{12}/ZrO_2

To understand the relation between structural diversity of designed catalysts and its activity, hydrogenation of styrene and cyclohexene were carried out under identical experimental conditions: (i) aqueous medium, 5 bar H_2 pressure for 3h at 30 °C, (ii) neat water, 5 bar H_2 pressure for 3h at 30 °C and (iii) neat water at 10 bar H_2 pressure for 2h at 50 °C, and the obtained results are shown in table 8, 9 and 10 respectively.

Table 8. Effect of Fe position in aqueous medium reaction at 5 bar H_2 pressure

Catalyst	Solvent	% Conversion	
		Styrene	Cyclohexene
$PMo_{11}Fe$	EtOH: H_2O (aqueous medium)	99	61
Fe-PMo_{12}/ZrO_2		97	73

Reaction conditions for aqueous medium: Active amount of Fe (0.020 mol%), substrate (9.87 mmol), EtOH: H_2O (30: 20 mL), H_2 pressure (5 bar), time (3 h) and temperature (30 °C).

Table 9. Effect of Fe position in neat water reaction at 5 bar H_2 pressure

Catalyst	Solvent	% Conversion	
		Styrene	Cyclohexene
$PMo_{11}Fe$	Neat H_2O	27	18
Fe-PMo_{12}/ZrO_2		29	24

Reaction conditions for neat H_2O: Active amount of Fe (0.024mol%), substrate (9.87 mmol), H_2O (50 mL), H_2 pressure (5 bar), time (2 h) and temperature (30 °C).

Table 10. Effect of Fe position in neat water reaction at 10 bar H_2 pressure

Catalyst	Solvent	% Conversion	
		Styrene	Cyclohexene
$PMo_{11}Fe$	Neat H_2O	83	76
Fe-PMo_{12}/ZrO_2		98	90

Reaction conditions for neat H_2O: Active amount of Fe (0.024 mol%), substrate (9.87 mmol), H_2O (50 mL), H_2 pressure (10 bar), time (2 h) and temperature (50 °C).

From the table 8, 9 and 10, it is seen that the designed Fe-PMo_{12}/ZrO_2 is more active for both styrene and cyclohexene hydrogenation as compared to $PMo_{11}Fe$. It can be explained on the basis of the nature of the substrate as well as the way it gets adsorbed on the catalytic active site. In other words, the structural diversity of substrate as well as position of catalytic active site in the catalyst play important role for the same.

It is well known that in heterogeneously catalyzed hydrogenation reactions, initially there is formation of metal hydride by dissociation of H_2. After that, the unsaturated reactant atoms coordinatively get adsorb on the formed metal hydride species. This activated species undergoes surface type reaction to produce reduced products, which subsequently gets desorbed from the catalyst surface.

As shown in figure 18, styrene consists of an allylic C=C bond while cyclohexene consist of cyclic C=C. In case of $PMo_{11}Fe$, it is easy for allylic C=C present in styrene to approach the active catalytic site of Fe (Fe-H) present in the lacuna. At the same time, it is difficult for the cyclic C=C present in cyclohexene to approach the active catalytic site of Fe present in the lacuna due to structural diversity of cyclohexene. However, in case of Fe-PMo_{12}/ZrO_2, Fe is present as counter cation position, and therefore it becomes easier for both allylic and cyclic C=C present in styrene and cyclohexene respectively to approach Fe (Fe-H). Due to these reasons, Fe-PMo_{12}/ZrO_2 is a better catalyst for cyclohexene hydrogenation.

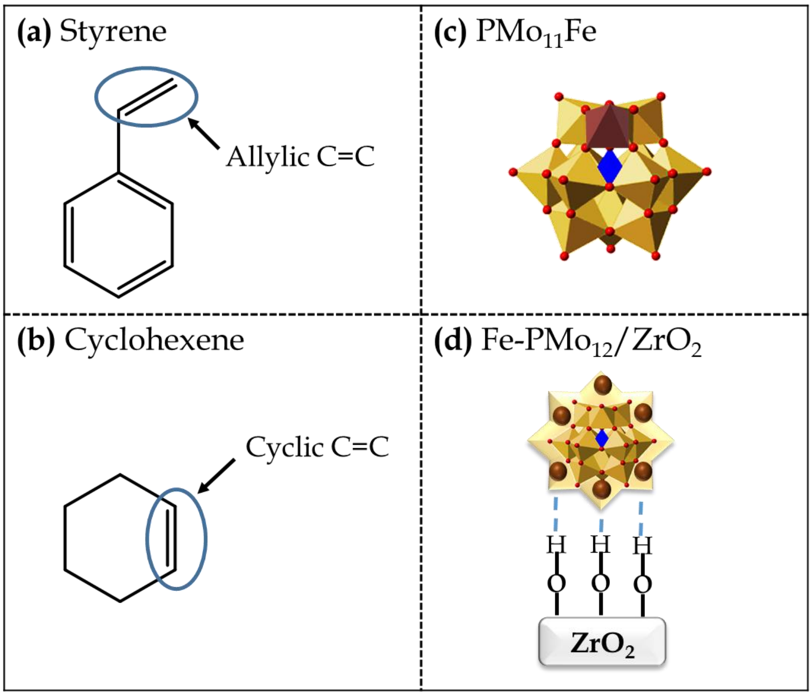

Figure 18. structure diversity of (a) styrene and (b) cyclohexene (c) $PMo_{11}Fe$ and (d) Fe-PMo_{12}/ZrO_2

Solvent also plays a crucial role for progress of the reaction. From table 8 and 9, it is seen that when the solvent is changed, the rate of reaction progress also changes because the solubility of the reactant is decreased which confirms that solvent plays an important role. In case of neat water (Table 9 and 10), Fe-PMo_{12}/ZrO_2 show high %conversion as compared to $PMo_{11}Fe$, in both the reaction conditions. The obtained result show high %conversion at 10 bar H_2 pressure at 50 °C as compared to reaction carried out using 5 bar H_2 pressure at 30 °C because at high temperature and pressure solubility of reactant is increased in water.

REFERENCES

[1] C. Avendaño, A. Briceño, F. J. Méndez, J. L. Brito, G. González, E. Cañizales, R. Atencio, P. Dieudonné, Dalton Trans., 42, 2822, (2013).

[2] M. Rohaniyan, A. Davoodnia, S. A. Beyramabadi, A. Khojastehnezhad, Applied Appl. Organomet. Chem., 33, e4881, (2019).

[3] W. Gao, X. Sun, H. Niu, X. Song, K. Li, H. Gao, W. Zhang, J. Yu, M. Jia, Microporous Mesoporous Mater., 213, 59, (2015).

[4] X. Zhang, Z. Zhang, B. Zhang, X. Yang, X. Chang, Z. Zhou, D.-H. Wang, M.-H. Zhang, X.-H. Bu, Appl. Catal. B: Environ., 256, 117804, (2019).

[5] Q. Zhang, X. Liu, T. Yang, C. Yue, Q. Pu, Y. Zhang, RSC Adv., 9, 8113, (2019).

[6] A. Patel, S. Pathan, Ind. Eng. Chem. Res., 51, 732, (2012).

[7] P. Sharma, A. Patel, J. Mol. Catal. A: Chem., 299, 37, (2009).

[8] X. Li, R. Cao, Q. Lin, Catal. Commun., 63, 79, (2015).

[9] X. Liu, J. Li, R. Wang, Chem. Eng. J., 316, 171, (2017).

[10] A. A. Bryzhin, M. G. Gantman, A. K. Buryak, I. G. Tarkhanova, Appl. Catal. B: Environ., 257, 117938, (2019).

[11] X. Song, W. Zhu, Y. Yan, H. Gao, W. Gao, W. Zhang, M. Jia, J. Mol. Catal. A: Chem., 413, 32, (2016).

[12] M. Abd El-Wahab, A. Said, J. Mol. Catal. A: Chem., 240, 109, (2005).

[13] B. Das, R. A. Kumar, P. Thirupathi, Y. Srinivas, Synth. Commun., 39, 3305, (2009).

[14] N. Narkhede, A. Patel, S. Singh, Dalton Trans., 43, 2512, (2014).

[15] S. Singh, N. Narkhede, A. Patel, RSC Adv., 5, 36270, (2015).

[16] G. S. Armatas, G. Bilis, M. Louloudi, J. Mater. Chem., 21, 2997, (2011).

[17] S. Mallik, S. S. Dash, K. M. Parida, B. K. Mohapatra, J. Colloid Interface Sci., 300, 237, (2006).

[18] P. Sharma, A. Patel, Appl. Surf. Sci., 255, 7635, (2009).

[19] S. Pathan, A. Patel, Dalton Trans., 40, 348, (2011).

[20] S. Pathan, A. Patel, Chem. Eng. J., 243, 183, (2014).

[21] S. Mallick, S. Rana, K. Parida, Ind. Eng. Chem. Res., 51, 7859, (2012).
[22] A. A. Ibrahim, S. M. Hassan, M. A. Mannaa, Colloids Surf. A Physicochem. Eng. Asp., 586, 124248, (2020).
[23] L. Shen, Y. Feng, H. Yin, A. Wang, L. Yu, T. Jiang, Y. Shen, Z. Wu, J. Ind. Eng. Chem., 17, 484, (2011).
[24] B. Maleki, H. Eshghi, A. Khojastehnezhad, R. Tayebee, S. S. Ashrafi, G. E. Kahoo, F. Moeinpour, RSC Adv., 5, 64850, (2015).
[25] N. M. Maksimov, N. N. Tomina, P. S. Solmanov, A. A. Pimerzin, Pet. Chem., 58, 1045, (2018).
[26] F. Gao, S. Ni, Z. Niu, X. Tang, H. Yi, C. Wang, J. Environ. Chem. Eng., 9, 106190, (2021).
[27] D. Yu, W. Gao, S. Xing, L. Lian, H. Zhang, X. Wang, D. lou, RSC Adv., 9, 4884, (2019).
[28] J. Xu, X. Cao, J. Xia, S. Gong, Z. Wang, L. Lu, Anal. Chim. Acta, 934, 44, (2016).
[29] J. Jiang, R. Zheng, Y. Jia, L. Guo, M. Huang, J. Hu, Y. Xia, Mol. Catal., 493, 111044, (2020).
[30] R. Eisavi, F. Ahmadi, Sci. Rep., 12, 11939, (2022).
[31] A. Patel, A. Patel, Catal. Lett., 149, 1476, (2019).
[32] S. Patel, N. Purohit, A. Patel, J. Mol. Catal. A: Chem., 192, 195, (2003).
[33] A. Patel, A. Patel, RSC Adv., 9, 1460, (2019).
[34] J. G. Hernández-Cortez, M. Manríquez, L. Lartundo-Rojas, E. López-Salinas, Catal. Today, 220-222, 32, (2014).
[35] H. Guo, G. Yin, J. Phys. Chem. C., 115, 17516, (2011).
[36] N. Mizuno, J. S. Min, A. Taguchi, Chem. Mater., 16, 2819, (2004).
[37] S. Haubenreisser, T. H. Wöste, C. Martínez, K. Ishihara, K. Muñiz, Angew. Chem. Int. Ed., 55, 1, (2016).
[38] B. Zhang, G. Sun, S. Ding, H. Asakura, J. Zhang, P. Sautet, N. Yan, J. Am. Chem. Soc., 141, 8185, (2019).

[39] H. Yu, G. Cao, F. Chen, X. Wang, J. Yu, M. Lei, Appl. Catal. B: Environ., 160-161, 658, (2014).

[40] P.-H. Phua, L. Lefort, J. A. F. Boogers, M. Tristany, J. G. de Vries, Chem. Commun., 3747, (2009).

[41] C. Rangheard, C. de Julián Fernández, P.-H. Phua, J. Hoorn, L. Lefort, J. G. de Vries, Dalton Trans., 39, 8464, (2010).

[42] M. Stein, J. Wieland, P. Steurer, F. Tölle, R. Mülhaupt, B. Breit, Adv. Synth. Catal., 353, 523, (2011).

[43] V. Kelsen, B. Wendt, S. Werkmeister, K. Junge, M. Beller, B. Chaudret, Chem. Commun, 49, 3416, (2013).